UCLA
UCLA Previously Published Works

Title

TREM2 macrophages induced by human lipids drive inflammation in acne lesions

Permalink

https://escholarship.org/uc/item/2800q59v

Journal

Science Immunology, 7(73)

ISSN

2470-9468

Authors

Do, Tran H
Ma, Feiyang
Andrade, Priscila R
et al.

Publication Date

2022-07-29

DOI

10.1126/sciimmunol.abo2787

Peer reviewed

TREM2 macrophages induced by human lipids drive inflammation in acne lesions

Tran H Do[1,2], **Feiyang Ma**[1,3], **Priscila R. Andrade**[2], **Rosane Teles**[2], **Bruno J. de Andrade Silva**[2], **Chanyue Hu**[3,4], **Alejandro Espinoza**[3,4], **Jer-En Hsu**[5], **Chun-Seok Cho**[5], **Myungjin Kim**[5], **Jingyue Xi**[6], **Xianying Xing**[7], **Olesya Plazyo**[7], **Lam C. Tsoi**[7], **Carol Cheng**[2], **Jenny Kim**[2], **Bryan D. Bryson**[8], **Alan M. O'Neill**[9], **Marco Colonna**[10], **Johann E. Gudjonsson**[7], **Eynav Klechevsky**[10], **Jun Hee Lee**[5], **Richard L. Gallo**[9], **Barry R. Bloom**[11], **Matteo Pellegrini**[3,4], **Robert L. Modlin**[2,12,*]

[1]Molecular Biology Institute, University of California Los Angeles; Los Angeles, CA 90095, USA

[2]Division of Dermatology, Department of Medicine, David Geffen School of Medicine; Los Angeles, CA 90095, USA

[3]Institute for Quantitative and Computational Biosciences - The Collaboratory, UCLA; Los Angeles, CA 90095, USA

[4]Department of Molecular Cell and Developmental Biology, University of California Los Angeles; Los Angeles, CA 90095, USA

[5]Department of Molecular and Integrative Physiology, University of Michigan Medical School, Ann Arbor, MI 48109, USA

[6]Department of Biostatistics, University of Michigan School of Public Health, Ann Arbor, MI 48109, USA

[7]Department of Dermatology, University of Michigan; Ann Arbor, MI 48109, USA

[8]Department of Biological Engineering, Massachusetts Institute of Technology; Cambridge, MA 02139, USA

[9]Department of Dermatology, University of California San Diego; La Jolla, CA 92093, USA

[10]Department of Pathology and Immunology, Washington University School of Medicine; St Louis, MO 63110, USA

*Corresponding author. rmodlin@mednet.ucla.edu.

[11]Department of Immunology and Infectious Diseases, Harvard T.H. Chan School of Public Health; Boston, MA 02115, USA

[12]Department of Microbiology, Immunology and Molecular Genetics, University of California Los Angeles, Los Angeles, CA 90095, USA

Abstract

Acne affects one in ten people globally, often resulting in disfigurement. The disease involves excess production of lipids, particularly squalene, increased growth of *Cutibacterium acnes*, and a host inflammatory response with foamy macrophages. By combining single-cell and spatial RNA-sequencing as well as ultra-high resolution Seq-Scope analyses of early acne lesions on back skin, we identified TREM2 macrophages expressing lipid metabolism and proinflammatory gene programs in proximity to hair follicle epithelium expressing squalene epoxidase. We established that the addition of squalene induced differentiation of TREM2 macrophages in vitro, which were unable to kill *C. acnes*. Notably, the addition of squalene to macrophages inhibited induction of oxidative enzymes and scavenged oxygen free radicals, providing an explanation for the efficacy of topical benzoyl peroxide in the clinical treatment of acne. The present work has elucidated the mechanisms by which TREM2 macrophages and unsaturated lipids, similar to their involvement in atherosclerosis, may contribute to the pathogenesis of acne.

One Sentence Summary:

Squalene induced proinflammatory TREM2 macrophages, a major cell type found in acne lesions, and blocked oxidative killing of *C. acnes*.

Introduction:

Acne affects more than 45 million people and is ranked third among chronic skin diseases that cause disability(1). Although common, the erythematous skin lesions and scarring in acne make the disease a major cause of psychosocial and psychological impairment in young people(2), triggering anxiety and mood disorders, affecting self-esteem(2–8), and leading to social isolation(7, 9, 10). Acne is estimated to lead to suicidal ideation in 7% of patients(11).

The pathogenesis of acne is characterized by increased production of lipids that are secreted as sebum by the pilosebaceous unit, which is formed by the epithelial lining of the hair follicle and sebaceous glands(12). The increased levels of sebum and the growth of the commensal *C. acnes*, along with obstruction of the hair follicle, contribute to severe inflammation resulting in the clinical manifestations of acne (13–15). As such, acne represents a common skin disease in which dysbiosis and its effect on the immune response contributes to pathogenesis(16).

The main lipid components of sebum include squalene, triglycerides, free fatty acids, wax esters, and cholesterol(14). These lipids can affect the growth of bacteria as well as the host immune response. Lipids that accumulate in the follicular duct are oxidized by a *C. acnes* lipase leading to bacterial proliferation(17). Squalene, a unique epidermal unsaturated

lipid in human sebum(14), is increased in acne patients(18). Its production is regulated by androgens(19), and hence coincides with the onset of acne at puberty. Squalene and its peroxides affect keratinocytes (KC)(20), T cells(21) and macrophages(13), which contribute to the development of acne lesions including the accompanying inflammation(22, 23). In addition, squalene is used as an adjuvant, MF59, in the FLUAD flu vaccine(24) and is being tested in some COVID-19 vaccine trials.

Foamy macrophages are abundant in acne lesions(25), as is typical of diseases of lipid metabolism, prominently in atherosclerosis(26), where they have been shown to express TREM2(27). The presence of foamy macrophages in diseases caused by *Chlamydia*(28), *Toxoplasma*(29), and *Mycobacterium*(30) species has indicated a link between lipid metabolism and microbes. The lipid metabolic products from these foam cells have been shown to trigger proinflammatory cytokines which amplify the inflammatory response(31). Yet the mechanisms and gene programs involved at the site of disease remain unclear. Since acne is a skin disease such that biopsy specimens can easily be obtained, acne provides an accessible model to investigate the interaction of lipid metabolism and inflammatory responses in humans.

To date, the level of study of acne has been limited to immunohistochemistry and global gene analysis(32, 33). Single-cell RNA sequencing (scRNA-seq) has emerged as powerful tool for delineating genetic and molecular profiles of individual cells, requiring few cells for analysis, so that it is possible to study transcriptional changes in specific cell types from disease lesions(34–37). Consequently, we sought to investigate the differences in immune function in acne at the single cell level to understand the interplay between host lipid metabolism, bacterial infection, and inflammation underlying the disease.

Results:

Cell Types Recovered in Lesional and Non-lesional Samples of Acne Patients

To elucidate cell heterogeneity and dynamic cellular changes in acne, we performed scRNA-seq using the 10X Genomics platform on early lesional (papules) and non-lesional skin from the back of six individuals with active acne vulgaris (Table S1). After removing RNA contamination by SoupX(38) and application of quality control filters using Seurat(34, 39) (Fig. S1a–b), we included a total of 32,966 cells from lesional skin and 29,202 cells from non-lesional skin for further scRNA-seq analysis. Gene expression data derived from cells in both lesional and non-lesional skin were aligned and projected onto a two-dimensional space using UMAP (Uniform Manifold Approximation and Projection)(34, 39). Unsupervised clustering revealed eight major clusters corresponding to seven different cell types (Fig. 1a, Table S2), with each cluster containing a mixture of lesional and non-lesional cells (Fig. 1b–c). Using differentially expressed genes and established canonical markers, we manually assigned cell type identities to endothelial cells, fibroblasts, lymphoid cells, smooth muscle, myeloid cells, two populations of keratinocytes (KC1 and KC2) and melanocytes (Fig. S1c). Within the myeloid, keratinocyte, fibroblast, and endothelial cell clusters, the cells from lesional versus non-lesional samples had distinct distributions (Fig. 1b). We failed to detect sebocytes, which may be related to the lack of a defined gene signature, cell lysis during processing of the biopsy specimen, and/or size exclusion during the cell capture.

We further sub-clustered and annotated the macrophages, keratinocytes, T cells, fibroblasts, and endothelial cell clusters. We then calculated the fraction of each cell type in individual samples and summed these fractions across all lesions and non-lesional samples. This showed that "Hair Follicle KC" and "TREM2 macrophages" were both abundant and more specific to acne lesional as compared to non-lesional skin (Fig. S1d).

We initially focused on the myeloid cluster, given that TREM2 macrophages were found to be one of the most abundant and specific sub-clusters in acne lesional vs. non-lesional skin and that myeloid cells are known to contribute to the pathogenesis of acne(40–42). The sub-clustering of the 2,638 myeloid cells identified six populations: three DC sub-clusters and three macrophage sub-clusters (Fig. 1d). The three DC sub-clusters were defined as CD1C^{+} DC, Langerhans cells (LC), and LAMP3^{+} DC (Fig. 1d, Fig. S2a–b, Table S3). We annotated two macrophage sub-clusters as M1-like macrophages and M2-like macrophages based on gene expression profiles for classically- (M1) and alternatively activated- (M2) macrophages(43–46) (Fig. 1d, Fig. S2a). The third and largest macrophage sub-cluster was identified as TREM2 macrophages(47–53), the cells of which are 95% associated with lesional skin (Fig. 1e–f). We searched for monocytes in the 4,370 total myeloid cells defined in the study by Casanova-Acebes et al. (54) across all sub-clusters, finding 145 *CD14^{+}VCAN^{+}S100A12^{+}* cells scattered throughout the CD1C^{+}DC and TREM2 macrophage sub-clusters. Of these, 38 cells were potentially monocytes, negative for the TREM2 macrophage markers (*APOC1*, *APOE*, *GPNMB* and *SPP1*) as well as the CD1c^{+} DC markers (*CD1C* and *CLEC10A*). We identified eight cells that were *CD16^{+}CD14^{−}* and negative for other macrophage markers, such that monocytes represented <1% of all myeloid cells. Similarly, in several scRNA-seq studies of healthy and inflammatory skin biopsy samples, a distinct monocyte subpopulation has not been identified(53, 55–58).

Given that KCs constitute approximately 90% of the cells in the epidermis, we sub-clustered the 8,271 KCs identifying five populations including spinous, basal, granular, eccrine gland, and hair follicle (Fig. 1g, Table S4). Using known keratin-specific markers, we categorized KCs as spinous KC (*KRT1, KRT10*), basal KC (*KRT5, KRT14*) and granular KC (*FLG* and *KRT2*) (Fig. S3a–b)(59–61). Cells localized to the eccrine gland were identified by *MUCL1* and *DCD*(61) were only found in non-lesional skin (Fig. S3b). The sub-cluster of KCs, which we designated as "hair follicle KC" based on its expression of *KRT6B* and *KRT6C,* was the most abundant and specific to acne lesional skin (Fig. S1d, S3b)(59, 62).

We found five sub-clusters of fibroblasts with two sub-clusters that are enriched in lesional cells (Fig. S4a–c, Table S5). Fibroblast sub-cluster 1, composed predominantly of cells derived from acne lesions, was characterized by expression of genes encoding metalloproteinases, consistent with microarray data of acne lesions (Fig. S4d–e)(32, 63). Fibroblast sub-cluster 5 was also derived from acne lesions and characterized by expression of *CCL19*. We found ten sub-clusters of endothelial cells based on their expression of *PECAM1* and *CDH5* that could be differentiated as arterial, venous or lymphatic, with sub-clusters identified as arterial and capillary predominantly derived from acne lesions (Fig. S4f–j, Table S6)(64). We detected five populations of lymphocytes including naïve/Th17 cells, naïve T cell(65), cytolytic T lymphocytes (CTL), regulatory T cells (Treg), NK cells, and B cells in both lesional and non-lesional skin that could be differentiated by expression

of signature genes, genes encoding cytokines and genes encoding cell surface markers (Fig. S5a–g, Table S7). We were not able to sub-cluster naïve/Th17 cells to separate out the Th17 cells, perhaps related to the low expression levels of Th17-related cytokines which may be due to the early nature of the lesions studied.

TREM2 Macrophages in Acne Lesions Express Lipid Metabolism and Inflammatory Genes

We focused on the role of TREM2 macrophage in acne because they were abundant in acne lesions as opposed to non-lesional skin (Fig S1d). We previously utilized scRNA-seq to examine the types of immune cells in a variety of inflammatory skin diseases(55). We reanalyzed the myeloid subpopulations in this dataset identifying that TREM2 macrophages were mainly derived from acne and leprosy lesions, and less frequent in biopsy samples from alopecia areata, granuloma annulare, healthy skin, and psoriasis (Fig. S6b). In a larger series of leprosy patients, we identified TREM2 macrophages in the lepromatous leprosy form of disease(66). In other studies of skin disease, TREM2 macrophages were not prominent in psoriasis (58, 67), atopic dermatitis (68) and vitiligo(67). In a reanalysis, macrophages expressing a TREM2 gene signature were detected in in atopic dermatitis lesions(69), comprising 4.4% of all macrophages from these lesions; in contrast, TREM2 macrophages account for 68.5% of all macrophages in acne lesions. A small number of TREM2 macrophages were found in resting hair follicles(52). Overall, TREM2 macrophages are found in inflammatory diseases in skin and other organs characterized by altered lipid metabolism in which foamy macrophages are a characteristic histologic feature.

To validate the expression of TREM2 in acne lesions, we performed immunohistochemistry, finding that TREM2 expression was greater in lesional acne biopsies compared to normal skin (Fig. S6c). By immunofluorescence staining, we showed that in acne lesions, TREM2 co-localized with CD68, a marker used to identify macrophages in inflammatory disease(70, 71) and TREM2 macrophages in disease lesions(72–74) (Fig. S6d). These results suggest that TREM2 macrophages accumulate in acne lesions.

We further evaluated the annotation of the TREM2 macrophages in acne lesions by comparing the sub-cluster signature to a curated set of 100 defined macrophage signatures from previously published studies including the seven scRNA-seq studies of TREM2 macrophages in diseases of altered limited metabolism(47–53) and the SAVANT database(75) (Table S8). The acne TREM2 macrophage sub-cluster was most similar to the three TREM2 macrophage signatures derived from microglia in Alzheimer's disease, foam cells in atherosclerosis and lung cancer macrophages(47–53) (Fig. S6e, Table S9). We derived a list of 26 conserved cluster signature genes that were present in at least four of the seven scRNA-seq studies reporting TREM2 macrophages (Table S10), finding that 19 genes were present in the TREM2 macrophage sub-cluster derived from acne lesions, with the others expressed by all the macrophage sub-clusters. The TREM2 macrophages in acne lesions expressed *APOE*, *SPP1*, *GPNMB*, *CTSD*, as well as *TREM2* (Fig. 2a), genes highly conserved among previous studies of these cells, thereby differentiating them from M1-like and M2-like macrophages. M1-like macrophages from lesional and non-lesional skin expressed similar levels of inflammatory cytokine genes including *IL1A*, *IL1B*, *TNF*, *IL6* and *IL12B* (Fig. S6A). Although we did not detect differences in other myeloid

subpopulations such as M1-like macrophages, our data do not exclude that other myeloid subpopulations contribute functionally to the pathogenesis of acne.

We performed KEGG pathway analysis of the top 100 signature genes in the acne lesion TREM2 macrophage sub-cluster, and found enrichment for pathways associated with lysosomes, cholesterol metabolism, mineral absorption, phagosome, and PPAR signaling (Fig. S7a, Table S11). Using gene ontology analysis, we identified 46 genes expressed as signature genes in TREM2 macrophages (Table S12) that are involved in cholesterol and lipid metabolism including lipid transport and binding, lipid intracellular transport, lipid signaling, lipid efflux, lipid storage, and lipid metabolism (Fig. 2b, Fig. S7a–b).

To measure the inflammatory capacity of the different cell populations, we divided each cell type and sub-cluster by lesional vs. non-lesional and summed z-scores for expression of each gene across cells of each type (see Methods). This analysis captures the total amount of each transcript by cell type allowing us to identify cells, in aggregate, that produce relatively more of a specific transcript than other cell types. Surprisingly, we found by Ingenuity analysis that 18 genes in the lesional cells of TREM2 macrophages with a z score 1.5 encoded "cytokines". These included proinflammatory chemokines and cytokines known to recruit and activate immune cells such as *IL18*, *CCL5*, *CCL18*, *CXCL2, CXCL3, CXCL5, CXCL9, CXCL16, MIF, SPP1, TNFSF13B,* and *TNFSF14*(76) (Table S13). We also detected expression of three members of the matrix metalloproteinase family members *MMP7*, *MMP9*, and *MMP12*, as well as two S100 family members *S100A8* and *S100A9 (*Fig. 2c, Fig. S7d–e). The acne TREM2 macrophage proinflammatory gene signature contained genes that were also upregulated in six of the seven scRNA-seq studies of TREM2 macrophage associated diseases (Table S14).

To map the directional trajectory of macrophage differentiation in acne lesions, we performed RNA velocity analysis(77, 78) on the cells in all myeloid sub-clusters. Using the rate of gene expression and the ratio of spliced and unspliced mRNA for an individual gene at any specific time point, we detected a linear trajectory from some M2-like macrophages to TREM2 macrophages as well as to CD1C^{+}DCs (Fig. 2d). No clear connection was found to the M1-like macrophages.

To further explore the relationship between TREM2 macrophages and M2-like macrophages, we used pseudotime analysis to align all 1,975 cells from these two sub-clusters onto a continuous trajectory (Fig. 2e). We found that the trajectory of M2-like and TREM2 macrophages lie along a largely polarized continuum given the overlap of some M2-like and TREM2 cells in the continuum (Fig. 2e). We detected four distinct gene patterns along the pseudotime trajectory (Table S15), which we interrogated using the 20 myeloid transcriptional subpopulations derived from scRNA-seq studies of lung(79). We found that Pattern A was associated with AREG^{+} myeloid cells, Pattern B with CD163^{+} macrophages, Pattern C with CXCL9^{+} myeloid cells and TREM2 macrophages, and Pattern D with SPP1^{+} macrophages (Fig. 2f, Fig. S8a–c). The module scores for these myeloid subpopulations sequentially changed during the pseudotime progression. A total of 19 of the 23 proinflammatory genes detected in the TREM2 macrophages from acne lesions were assigned to the pseudotime trajectory, with eight genes each present in Patterns C and D

(Fig. S8d). Three of the proinflammatory genes in pattern C that were robustly expressed, *CCL18*, *IL18* and *S100A8*, were detected in cells expressing the nine gene TREM2 score within the TREM2 macrophage sub-cluster (Fig. 2g). These data suggest a trajectory linking M2-like to TREM2 macrophages, characterized by the increased expression of proinflammatory genes in the TREM2 macrophages.

To further validate the expression of inflammatory genes in the TREM2 macrophages, we reanalyzed the scRNA-seq data for human myeloid cells isolated from adipose tissue(48), identifying five subpopulations including one characterized by robust expression of *TREM2* and a second with lower expression of *TREM2* (Fig. S9a–b). We overlapped the signature genes from TREM2 macrophages in adipose tissue(48) with TREM2 macrophages in acne lesions, finding that there are 157 signature genes shared between the two macrophages (Table S16), including 23 lipid transport and metabolism genes as well as 15 inflammatory genes including five inflammatory genes in the published cluster markers(48): *CCL18*, *CXCL16*, *IL1RN*, *SPP1* and *MMP9* (Fig. S9c–d, Table S16, S17). Of the 18 inflammatory genes we found to be increased in TREM2 macrophages in acne lesions by z score analysis, eight were significant cluster marker genes, with four ranked in the top 22 (Fig. S9f). By contrast, we found only two of the inflammatory genes from acne TREM2 macrophages were significant cluster marker genes for the TREM2 macrophages in murine resting hair follicles(52), and neither was ranked in the top 50 (Fig. S9f). This is consistent with a model in which there is a spectrum of TREM2 macrophages that express varying levels of inflammatory genes that may contribute to inflammation in acne and obesity and to homeostasis in the resting hair follicle(52).

KCs in the Hair Follicles in Acne Lesions are Capable of Squalene Synthesis

As hair follicle KC are part of the pilosebaceous unit, we investigated their gene expression for genes involved in the key components of human sebum. This sub-cluster highly expressed squalene pathway genes such as *FDFT1* (squalene synthase) and *SQLE* (squalene epoxidase) (Fig. 3a)(80). We did not observe any upregulation of genes for fatty acid synthesis(81), wax ester synthesis(82), triglyceride synthesis(83), or cholesterol synthesis(80) (Fig. S10). SQLE and FDFT1 protein expression was detected by immunohistochemical staining in hair follicle keratinocytes (black arrow) and sebocytes (yellow arrow) in acne lesions. (Fig. 3b). SQLE expression was greater in acne lesions compared to healthy skin in both the hair follicle keratinocytes and sebocytes. FDFT1 expression was greater hair follicle keratinocytes in acne lesions compared to healthy skin and detected in sebocytes in both specimen types.

Spatial and Seq-scope sequencing spatially localize cell populations in acne

To localize the key cell types we identified in acne lesions by scRNA-seq, we performed spatial-seq(84) on an acne skin biopsy specimen. We were able to collect RNA from a 20μm thick frozen section of an acne lesion into 55μm wells containing spatially-barcoded capture oligonucleotides and performed transcriptome analysis. We detected 394 spatially defined spots with an average of 1,349 genes and 2,950 transcripts per spot. The acne biopsy specimen contained a hair shaft in the center of epidermis surrounding by an epithelial lining as well as a perifollicular inflammatory infiltrate (Fig. 3c). We annotated the

cell-type composition for each spot by deconvoluting the spatial gene expression using the scRNA-seq gene expression of the major cell-types, displayed as a scatter-pie plot, which contains a pie chart for each spot scattered across the spatial array. As expected, the spots overlying the epidermis mostly contained cells expressing a keratinocyte signature. Spots that were identified as containing mostly myeloid cells were located near the hair follicle and throughout the papillary dermis, with focal aggregates in the deeper reticular dermis. The other spots in the acne biopsy specimen contained mixtures of several cell types (Fig. 3c).

We derived a gene signature score from the hair follicle KC scRNA-seq cluster comprised of *KRT6C*, *KRT6B* and *KRT17*. This hair follicle gene score identified the spots overlying the hair follicle in the biopsy specimen (Fig. 3c). Using a two-color spatial plot, we demonstrate that *SQLE* was expressed by the hair follicle, and this was in proximity to spots identified with a TREM2 macrophage nine gene score (Fig. 3c). The proximity of spots expressing *SQLE* and the TREM2 macrophage nine-gene score was confirmed in two additional acne lesional samples (Fig. S11a). Additional TREM2 macrophages were located in the areas of inflammatory infiltrate in the deeper dermis distal from the *SQLE* expression.

We validated the spatial-seq localization of *SQLE*- and *TREM2*- encoded proteins by immunohistochemistry (Fig. 3b). Squalene epoxidase was most strongly expressed in the hair follicle epithelium and in the sebaceous gland. TREM2^{+} cells (red arrow) were abundant in the area surrounding the hair follicle epithelium and sebaceous glands in acne lesions and difficult to detect in healthy skin. There were few positive cells for squalene epoxidase and TREM2 in healthy skin (Fig. 3b).

We more precisely defined the microanatomic location of TREM2 macrophages to the hair follicle in an acne lesion using Seq-Scope(85), which allows the measurement of gene expression in tissue at an ultra-high resolution, using as low as 0.5 μm spot-to-spot resolution, compared to the 100 m spot-to-spot resolution of the 10X Visium platform. This biopsy specimen contained a hair follicle in longitudinal section surrounded by an inflammatory infiltrate (Fig. 3d). We segmented the histology area with 10 m-sided square grids, which revealed an average of 145 genes and 167 transcripts across 3,558 grids in an acne lesion. We clustered and annotated the 10 m grid dataset using the cluster and sub-cluster signature genes from the acne scRNA-seq dataset, defining the location of TREM2 macrophages, other macrophages, KRT5^{+} and KRT16^{+} keratinocytes, fibroblasts, endothelial, and B cells. We then further refined the spatial resolution of the dataset by transferring the annotations obtained under 10 m grids to the sliding-grid datasets with 5 m, 2 m and 1 m intervals between the center of two adjacent grids. KRT5^{+} keratinocytes were identified in the basal layer of the epidermis and the outer root sheath of the hair follicle, whereas KRT16^{+} keratinocytes were identified in the inner root sheath of the hair follicle (Fig. 3d). TREM2 macrophages, other macrophages and fibroblasts were localized in close proximity as well as directly adjacent to the hair follicle. A magnified view of the region near the hair follicle at 1 m resolution identifies TREM2 macrophages adjacent to KRT5^{+} keratinocytes in the hair follicle outer root sheath (Fig. 3d inset). We also plotted the expression of individual genes, confirming the microanatomic location of *KRT5* and *KRT16* expression, with the localization of *APOE*, a key marker of TREM2 macrophages in the area

surrounding the hair follicle (Fig. 3e) as well as *APOC1, CCL18, GPNMB*, and *LIPA* (Fig. S11b).

Using a monoclonal antibody to the *C. acnes* lipoteichoic acid(86), we detected bacterial antigen in and around the hair pilosebaceous unit. TREM2^{+} cells were also present near the hair follicle. By immunohistochemistry and confocal microscopy, we colocalized *C. acnes* antigen with TREM2 macrophages proximal to the hair follicle (Fig. 3f, Fig. S11c–e). There was some background TREM2 labelling of the epidermis, as is often seen with immunohistology of skin, but little *C. acnes* antigen and few TREM2^{+} cells in normal skin. These data indicate that TREM2 macrophages containing *C. acnes* antigens are located near hair follicle epithelium expressing squalene oxidase.

Squalene Induces TREM2 Expression in Macrophages In Vitro

In order to develop an in vitro model of TREM2 macrophages in acne lesions, we used Ingenuity Pathway Analysis (IPA) to analyze the TREM2 macrophage cluster markers to identify cytokines that were upstream regulators and therefore could drive the differentiation of TREM2 macrophages. The top five upstream regulators identified were *IFNG, IL13, TNF, IL1B,* and *IL4.* Of these, IL-4 has been reported, in combination with macrophage colony-stimulating factor (M-CSF), to induce TREM2 expression in macrophages in vitro(87). We tested these cytokine candidates, with and without M-CSF, for their ability to induce TREM2 expression on adherent macrophages in vitro (Fig. 4a). We also tested the ability of squalene to induce TREM2 expression given that squalene synthase expression was upregulated in hair follicle KCs in proximity to TREM2 macrophages. Culture of five-day M-CSF derived macrophages with IL-4 or squalene in the presence of M-CSF markedly upregulated TREM2 expression compared to M-CSF alone (Fig. 4a, Fig. S12a). The addition of squalene induced TREM2 expression in macrophages in a dose-dependent manner (Fig. S12b). Among other components of sebum(21), lauryl palmitoleate induced TREM2 expression in a dose-dependent manner, palmitoleic acid induced TREM2 expression only at the lowest concentration tested, and cholesterol did not induce TREM2 in macrophages (Fig. S12c).

To validate that the squalene-derived TREM2 macrophages represent an in vitro model for the TREM2 macrophages in acne lesions, we compared the expression of key lipid transport and metabolism genes. The lipid efflux transporters *ABCA1* and *APOE*, and fatty acid metabolism enzyme *LPL,* the cytokine and lipid metabolism regulator *SPP1*, as well as the lipid sensor *TREM2* are significantly upregulated in squalene/M-CSF-treated macrophages compared to the IFN-γ/LPS treated macrophages which serve as a model for M1-like macrophages(88) (Fig. 4b, Fig. S2d), paralleling the differential expression observed in TREM2 macrophages from acne lesions.

We also analyzed scRNA-seq data obtained from M-CSF and squalene/M-CSF-treated macrophages and identified ten total clusters (Fig. S13a). In all cells, the expression for the top ten signature genes derived from the TREM2, M1-like and M2-like macrophages in acne lesions was determined. This revealed that the in vitro derived macrophages had a higher signature score for TREM2 like macrophages than the M1-like or M2-like macrophages

(Fig. 4c). We computed the top 10 gene signature scores of the acne lesion macrophages for the in vitro macrophage sub-clusters. We found four sub-clusters with the highest TREM2 scores, clusters 1, 3, 7 and 8 (Fig. S13b), and therefore consider these the most TREM2-like macrophages. We observed that these TREM2-like sub-clusters are enriched for the squalene treated cells (Fig. S13c), suggesting that squalene treatment drives more macrophages into a TREM2 like state than M-CSF alone. Thus, the squalene-derived TREM2 macrophages provide a reasonable model for the TREM2 macrophages in acne lesions

The squalene/M-CSF treated macrophages were replete with lipids as measured by BODIPY, as compared to IFN-γ/LPS treated M1-like macrophages (Fig. 4d). We found squalene/M-CSF macrophages have enhanced phagocytosis of latex beads and *C. acnes* compared to IFN-γ/LPS treated and M-CSF treated macrophages (Fig. S12d–e). Squalene/M-CSF macrophages had little antimicrobial activity against *C. acnes* (Fig. S12f). We also observed that live *C. acnes* stimulates squalene/M-CSF macrophages to secrete IL-18 at a similar level to IFN-γ/LPS macrophages (Fig. S12g), consistent with the expression of *IL18* in TREM2 macrophages in acne lesions (Fig. S7d–e). We also found *IFNG* to be differentially expressed in CTLs from lesional compared to non-lesional skin (Fig. S5g). Given the ability of IL-18 to induce IFN-γ, the expression of *IL18* in TREM2 macrophages in acne lesions and the in vitro secretion of IL-18 by TREM2 macrophages cultured with *C. acnes* suggest a possible inflammatory role for TREM2 macrophages in acne.

Squalene Blocks Oxidative Killing of C. acnes

Given the ability of M1-like macrophages to mount an antimicrobial response against *C. acnes(89)*, we compared the antimicrobial response of IFN-γ/LPS macrophages and squalene-derived TREM2 macrophages. The IFN-γ/LPS macrophages exhibited a greater antimicrobial response against *C. acne* strains of phylotype IA_1 derived from acne lesions than strains of phylotype II derived from healthy skin (Fig. 4e). In comparison, squalene-derived TREM2 macrophages showed little antimicrobial activity (Fig. 4e). We asked whether squalene affects the antimicrobial activity of macrophages by deriving IFN-γ/LPS macrophages in the presence or absence of squalene infected with *C. acnes*, then comparing the number of viable bacilli by CFU assay at 24 hours. We found that the addition of squalene decreased the antimicrobial activity of IFN-γ/LPS macrophages against *C. acnes* from 80% to 30% (Fig. 4f). The antimicrobial activity of M-CSF derived macrophages was significantly less than IFN-γ/LPS macrophages, and further reduced by the addition of squalene (Fig. 4f).

Squalene consists of a methyl group attached to six double bonds that act as a highly effective reactive oxygen species (ROS) scavenger with a rate constant much larger than other lipids on human skin(90). Squalene has also been found to reduce intracellular ROS as well as UV-induced ROS levels in cultured cells(91). Macrophages employ ROS and reactive nitrogen intermediates (RNI) in phagosomes to kill intracellular pathogens(92). To investigate which intermediates have antimicrobial activity against *C. acnes*, we employed the NO-donor Diethylenetriamine NONOate (DETA NONOate) and two oxygen donors, alkyl peroxide tertiary-butyl hydroperoxide (TBHP) and hydrogen peroxide (H_2O_2). *C. acnes* was more sensitive to killing by ROS as compared to DETA NONOate (Fig. 4g).

Squalene was able to block the killing of *C. acnes* in the presence of TBHP at similar efficacy to the oxygen scavenger N-acetyl cysteine (NAC), which served as a control (Fig. 4h).

We next asked whether squalene modulates the antimicrobial gene expression profile of macrophages. In IFN-γ/LPS macrophages, squalene reduced the expression of genes encoding the oxidative enzymes that produce ROS and RNI including NADPH oxidase *NOX1*, *NOS2* (inducible nitric oxide synthase, iNOS), and *NFKB*(93) (Fig. S14), but not *NOX4*. Squalene also reduced the expression of genes encoding ROS-inducible oxidative pathway enzymes including mitogen-activated protein kinases *MAPK8* (c-Jun NH2-terminal kinase-JNK), *MAPK14* (p38 MAPK) and *NFKB*(93) (Fig. S14), consistent with the inhibition of ROS production.

Together, these data suggest that squalene, which is overproduced in acne lesions, induces TREM2 macrophages with enhanced phagocytic capacity for lipids and *C. acnes,* but scavenges oxygen radicals thus blocking the macrophage antimicrobial response. These TREM2 macrophages are not able to reduce the bacterial load, but secrete IL-18 and upregulate chemokine expression, thus contributing to the inflammation that is characteristic at the site of disease (Fig. 5).

Discussion:

TREM2 macrophages have been shown to be present at the site of a variety of metabolic diseases characterized by alterations in lipid metabolism and the presence of chronic inflammation. These diseases involve the cardiovascular system, adipose tissue, liver, and brain, such as atherosclerosis, obesity, Alzheimer's disease, and non-alcoholic fatty liver(47–53). The TREM2 macrophages in these diseases are likely identical to the foamy macrophages that are characteristic of these conditions(27). Unexpectedly, TREM2 macrophages were a major cell type infiltrating acne lesions, consistent with the presence of foamy macrophages containing lipid droplets in acne lesions(25). We found eight lipid metabolism associated genes (*APOE, CTSB, TREM2, LPL, LGALS3, CTSD, LIPA,* and *NPC2*) that were present in acne TREM2 macrophages as well as the majority of seven scRNA-seq studies of TREM2 macrophages in metabolic disease. While it remains to be determined what proportion of the foamy macrophages in acne express TREM2, our data indicates that the pathogenesis of acne shares features of other metabolic diseases in which TREM2 macrophages and lipid dysregulation are prominent.

A key finding of the present study is that squalene induced TREM2 expression on monocyte-derived macrophages, resulting in expression of a similar lipid metabolic and inflammatory gene program as the TREM2 macrophages in acne lesions. Squalene was differentially increased in the sebum in skin of acne patients as compared to healthy controls(18). Squalene-induced TREM2 macrophages accumulate lipids, as confirmed by visualization of lipid droplets in the cytoplasm by fluorescence staining for neutral lipids, similarly to the foamy macrophages detected in acne lesions(25). This is consistent with the reported ability of squalene to induce *ABCA1*, and *APOE* expression in murine macrophages(94), with both of the encoding genes part of the acne TREM2

macrophage gene signature. TREM2 regulates cholesterol metabolism and transport(95). Other components of sebum, lauryl palmitoleate (LP) and palmitoleic acid (PA), but not cholesterol, induced TREM2 expression on macrophages. The production of squalene, increased in acne patients (18), is linked to the pathogenesis of acne, as androgens, which trigger acne, induce squalene synthesis via sterol regulatory element binding proteins (SREBPs)(19). A diet high in the polyunsaturated oleic and linoleic acids was sufficient to induce TREM2 expression in Kupffer cells in mice(96). In addition to lipids, only the Th2 cytokines IL-4 and IL-13 have been shown to induce TREM2 expression in vitro(87). By cell fate analysis(54), TREM2 macrophages in tissue have been shown to derive from monocytes, however, we found few monocytes in acne lesions. Alternatively, we provide evidence from RNA velocity analysis that some TREM2 macrophages derive from M2-like macrophages. Our data provides a mechanism by which squalene in sebum alters the inflammatory cell types that accumulate in skin. To more effectively study the role of squalene in inducing TREM2 macrophages in vitro, it would be useful to have an appropriate animal model; however, squalene is present in human but not mouse sebum(14).

In proximity to TREM2 macrophages in acne lesions, we found by spatial-seq and immunohistochemistry that hair follicle keratinocytes expressed squalene epoxidase, an enzyme that converts squalene into squalene epoxide, a polyunsaturated lipid that is known to scavenge ROS(90), but can also directly trigger inflammatory responses(20). Seq-Scope, which provides an ultra-high submicrometer resolution(85), further revealed the details of spatial context where TREM2 macrophages were situated. TREM2 macrophages were detected in close proximity to the acne lesion hair follicle and were intermingled with other cell types involved in inflammation, such as fibroblasts, B cells, and other macrophages. In skin, TREM2 macrophages have been identified at a low frequency in the resting hair follicle(52) and found to accumulate within the granulomas of the progressive form of leprosy(66). We found that squalene-induced TREM2 macrophages were phagocytic for *C. acnes* but were unable to kill the bacterium. Squalene abrogated the ability of IFN-/ LPS-activated macrophages to effectively mount an antimicrobial response against *C. acnes*. We determined that oxygen radicals killed *C. acnes* more potently than nitrogen radicals in axenic culture. Squalene blocked the antimicrobial response against *C. acnes* by inhibiting the generation of ROS and scavenging oxygen free radicals, consistent with Chapman's observations in 1917(97) and 1923(98) that squalene isolated from shark oil is an ROS scavenger. These data provide a novel mechanism in which the excess production of the lipid, squalene, contributes to the pathogenesis of acne by inducing TREM2 inflammatory macrophages and blocking antimicrobial responses. It remains to be determined whether squalene, which is a polyunsaturated hydrocarbon ($C_{30}H_{50}$), is directly active or must be metabolized for this effect. The TLR1/2 ligand, PAM_3CSK_4, has been shown to induce *SQLE* in sebocytes in vitro(99), providing a mechanism for how *C. acnes* could affect squalene metabolism.

Our data provide evidence, previously unappreciated, that TREM2 macrophages contribute to inflammation, by finding that the TREM2 macrophages in acne lesions expressed 23 proinflammatory genes. Of these, 15 were expressed in at least one of the seven scRNA-seq studies of TREM2 macrophages in metabolic disease. A key gene upregulated in acne lesions encodes IL-18, which we validated to be produced by squalene-induced TREM2

macrophages in vitro. Along with IL-18, another molecule found to be upregulated in acne TREM2 macrophages, MMP-9, is present in the sebum of acne patients(100) and cleaves IL-1β into the biologically active form(101). IL-18 acts with IL-12 to enhance production of a key proinflammatory cytokine IFN-γ by NK and Th1 cells(102–104). Squalene has also been shown to stimulate macrophages to increase IL-1β secretion(13), consistent with the role of squalene in modulating the inflammatory response. The M1-like macrophages in acne lesions differentially expressed *IL12B* compared to macrophages from non-lesional skin. The local production of IL-12 may be stimulated via LAMP3^{+} DC production of CCL17 in acne lesions(105, 106). Concordantly, we found IFN-γ to be differentially expressed in CTLs from acne lesions compared to uninvolved skin. *SPP1*, also upregulated in TREM2 macrophages in acne lesions, encodes secreted phosphoprotein-1, a potent chemoattract for macrophages and can augment the production of IL-12 while inhibiting production of IL-10(107). *SPP1* was upregulated in five out of the seven TREM2 macrophage scRNA-seq studies and is known to be induced by oxidized LDL in macrophages(108). *CXCL16,* upregulated in TREM2 macrophages in acne lesions, and found in four out of seven studies of TREM2 macrophages in the literature, encodes a chemokine that is a chemoattractant for NKT and innate lymphoid cells (ILCs) in the skin, and can act as scavenger receptor for oxidized LDL(109). TREM2 macrophages are not typically present in inflammatory skin diseases, as they were not prominent in scRNA-seq data from psoriasis(58, 67), atopic dermatitis(68) and in our reanalysis of myeloid cells in a variety of inflammatory skin diseases(55). Thus, from studying acne, we identified a general feature of some TREM2 macrophages, namely their contribution to inflammation in metabolic disease. However, TREM2 macrophages may contribute to homeostasis in resting hair follicles(52), immunosuppression in cancer(110) and progressive infection in leprosy (66), such that studies are needed to characterize the functional spectrum of TREM2 macrophage responses in different disease states.

Our findings provide insights for effective therapy of acne. Clearly, squalene is one determinant of pathogenesis that induces TREM2 inflammatory macrophages and blocks oxidative killing of *C. acnes*. Perhaps topical treatment of acne with the oxygen radical producer benzoyl peroxide can overcome oxygen radical scavenging properties of squalene. Retinoids, also effective in the treatment of acne, inhibit sebum production including squalene in skin. In addition, antifungal agents which inhibit squalene epoxidase have been shown to ameliorate acne(111). Finally, recent evidence suggests that statins, which block the synthesis of mevalonate, a precursor of squalene, have therapeutic efficacy in reducing lesions(112). Our findings suggest that the TREM2 macrophages represent a general and conserved response to dysregulation of lipid metabolism. Accumulation of intracellular lipids promotes the upregulation of proinflammatory cytokines and chemokines in macrophages, which contributes to the immunopathology of these diseases. By finding that diseases with seemingly different etiologies such as atherosclerosis, obesity, Alzheimer's disease, and non-alcoholic fatty liver disease, share the presence of TREM2 macrophages with a conserved inflammatory signature, the present study suggests that these cells may represent common targets for intervention to mitigate the inflammation-induced tissue injury characteristic of metabolic disease.

Materials and Methods:

Study design

The goal of this study was to provide mechanistic insight into the relationship between different cell types in acne lesions, of which TREM2 macrophages were a predominant lesional cell type. To do so, we performed scRNA-seq and spatial-seq on active acne lesions and non-lesional skin of the same individuals. To validate our scRNA-seq findings, we performed immunohistology on acne lesions which identified the proximity of TREM2 macrophages to hair follicle keratinocytes capable of producing squalene. We performed in vitro experiments on macrophages to investigate the effects of squalene on the expression of TREM2 and the function of the macrophage antimicrobial activity against *C. acnes*. We also used axenic *C. acnes* cultures to dissect the mechanisms underlying the effect of squalene on antimicrobial activity.

Skin samples and processing of human skin

The study was performed in accordance with protocols approved by the institutional review board at University of California, Los Angeles. All patients provided written informed consent. Acne donors were recruited from the University of California, Los Angeles. Patients were excluded from the study if they had been using acne medication, hormonal regulation medication, or hormonal-related implants in the past three months. Skin samples were obtained from 4-mm punch biopsies of early (< 24hour) papules on the back. Sample processing were as previously described(66). Briefly, skin was digested enzymatically at 2 hours with 0.4% Dispase II at 37°C with agitation. The epidermis was separated from the dermis. Epidermis was then treated with 0.25% Trypsin and 10U/mL of DNAse I for 30 minutes. Dermis was homogenized and treated with 0.4% Collagenase II and 10U/mL DNase I for 2 hours. The digested samples were filtered through a 70 μm cell strainer and washed with 5ml of RPMI (Gibco, cat. # 11875093). The digested cells were centrifuged at 300g for 10 mins at 4°C. After discarding the supernatant, the cells were suspended in 1mL of RPMI and counted. Live cells were counted using 0.4% trypan blue (Gibco, cat. # 15250061). If the cell viability was above 80%, we loaded isolated cells onto the Chromium instrument (10X Genomics) according to the Chromium Single Cell 3' Reagent Kit v3 user guide.

Immunohistochemical and immunofluorescence staining

Formalin-fixed, paraffin-embedded tissue slides obtained from papules of acne patients and healthy skin from the scalp were heated for 30 min at 60°C, deparaffinized, and rehydrated. We used healthy skin from the scalp to evaluate the protein expression in sebaceous glands that would otherwise be difficult to isolate in normal skin. Slides were placed in antigen retrieval buffer and heated at 125°C for 3- seconds in a pressure cooker water bath. After cooling, slides were blocked using 10% Donkey serum (30 minutes). Overnight co-incubation (4°C) was then performed using anti-human TREM2 at 0.5mg/ml (ThermoFisher Scientific, cat. #PA5–18763), anti-FDFT1 at 0.93mg/ml (1:150) (ThermoFisher Scientific, cat. # MA5–25676) and anti-SQLE (Fisher Scientific, cat. # PA5–54265). Images presented are representative of at least three biologic replicates.

Cryosections (4mm) from acne patients were incubated with antibodies against CD68 (Invitrogen, cat # MA5–13324) followed by Alexa Fluor 594 isotype specific secondary (Invitrogen, cat. # A21125). Sections were washed, incubated with monoclonal antibody for TREM2 (Novus Biologic, cat. # NBP1–07101), followed by Alexa Fluor 647 isotype-specific secondary (Invitrogen, cat. # A21240). Similarly, other 4mm cryosection of skin were incubated with antibodies against TREM2 at 0.5mg/ml (ThermoFisher Scientific, cat. #PA5–18763) followed by Alexa Fluor 594 isotype, washed as above, followed by *C. acnes* monoclonal antibody (PAB antibody) (MBL Bio, cat# D371–3), and stained with Alexa Fluor 647. Slides were mounted in crystal mounting medium (Biomedia) and then preserved with Prolong Gold with DAPI (Invitrogen, cat. # P36931). Immunofluorescence of skin sections were examined using a Leica-TCSSP MP inverted single confocal laser-scanning and a two-photon laser microscope (Leica, Heidelberg, Germany). Colocalization analysis was performed with Leica Application Suite X (LAS X).

In vitro M-CSF derived macrophage characterization

The study was performed in accordance with protocols approved by the institutional review board at University of California, Los Angeles. All patients provided written informed consent. Healthy donors were recruited from the University of California, Los Angeles. Peripheral blood mononuclear cells (PBMCs) from healthy donors were isolated from peripheral blood using a Ficoll-Paque (GE Healthcare) density gradient. Monocytes were isolated from PBMCs by adherence for 2 hours with RPMI supplemented with 1% fetal calf serum (FCS) or via positive selection with CD14 microbead (Miltenyi Biotec, cat# 130–050-201). Monocytes were seeded at 500,000 cells/well in a 24-well plate and differentiated in M-CSF (50 ng/ml) (R&D Systems, cat. # 216MC025/CF) for 5 day in RPMI with 10% FCS at 37°C.

To evaluate in vitro derived macrophages for TREM2 expression, TNF- (10ng/ml) (Thermo Scientific, cat.#PHC3015), IFN-γ (100 ng/mL) (BD, cat. # 554617), IL-4 (20ng/mL) (Peprotech, cat. # 200–04), IL-1β (1 ng/mL) (Thermo Scientific, cat. # PHC0815), squalene (1 mM) (Thermofisher Scientific, cat.# S3626–100ML), cholesterol (0.025 mM, 0.25 mM, 0.5 mM) (Sigma, cat. # C8667), lauryl palmitoleate (10 mM, 100 mM, 200 mM) (Santa Cruz Biotechnology, cat # 108321–49-9), and palmitoleic acid (10 mM, 100 mM, 200 mM) (Cayman Chemical, cat# 10009871) were added with and/or without M-CSF (50 ng/ml) (R&D Systems, cat. # 216MC025/CF) to above M-CSF derived macrophages for 2 days. Lipids (squalene, cholesterol, lauryl palmitoleate, and palmitoleic acid) were sonicated for 30 minutes in RPMI prior to adding to macrophage culture. TREM2 expression were evaluated via flow cytometry. Adherent cells were detached with 1mM EDTA in PBS. Cells were stained with APC-conjugated mAbs against TREM2 (R&D Systems, cat. #FAB17291A). Isotype controls were performed in parallel. Cells were acquired with LSR II flow cytometer (BD) and analyzed with FlowJo (BD).

For evaluation of RNA from in vitro derived macrophages, 5-day M-CSF derived macrophages (described above) were stimulated with LPS (100ng/mL) (Enzo, cat. # ALX-581–007-L001) + IFN-γ (20ng/mL) (BD, cat. # 554617) for M1-like macrophages as well as M-CSF (50 ng/ml) (R&D Systems, cat. # 216MC025/CF) and squalene (1

mM) (Thermofisher Scientific, cat.# S3626–100ML) were differentiated for 1 day for squalene/M-CSF macrophages. Macrophages were extracted after 24 hours with stimuli (described above) and further evaluated with quantitative PCR or scRNA-seq analyses.

RNA isolation and reverse transcription-real time quantitative PCR analysis

Total RNA were isolated at 12 hours and 24 hours using TRIzol (Invitrogen) according to manufacturer's protocol. First strand cDNA synthesis was performed with iScript cDNA synthesis kit (BioRad, cat. # 1708891). Total RNA were subjected to reverse transcription-quantitative polymerase chain reaction (RT-qPCR) via Bio-Rad IQ5 system using iQ SYBR Green Master Mix 2X (Kapa Biosystems, cat. # KK4618). The relative quantities of gene tested per sample were calculated against GAPDH using   Ct. Human specific probes were generated by RT-qPCR amplification using the primer sets provided in the Supplemental Materials.

In vitro M-CSF derived macrophage single cell processing

In vitro 5-day M-CSF derived macrophages were stimulated with either M-CSF (50 ng/ml) (R&D Systems, cat. # 216MC025/) and/or squalene (1 mM) (Thermofisher Scientific, cat.# S3626–100ML). These macrophages were separated from culture plates with trypsin-EDTA and filtered through a 70 μm cell strainer and washed with 1ml of RPMI (Gibco, cat. # 11875093). The macrophages were centrifuged at 300g for 10 mins at 4°C. After discarding the supernatant, the cells were suspended in 1mL of RPMI and counted. Live cells were counted using 0.4% trypan blue (Gibco, cat. # 15250061). If the cell viability was above 90%, we loaded isolated cells onto the Chromium instrument (10X Genomics) as described above. Single cell RNA-seq sequencing, alignment, and analyses are described above.

Fluorescence microscopy for neutral lipid visualization

Adherent macrophages were removed from culture plates with trypsin-EDTA and plated onto poly-L-lysine coated printed slides. Cells were then fixed with 4% paraformaldehyde for 10 minutes and washed twice with PBS. For lipid droplet visualization, cells were permeabilized 0.1% Triton X-100 (Sigma, cat# X100) and incubated with 4ug/mL BODIPY 493/503 (Thermofisher cat. D3922) for 1 hour at room temperature. Slides were then preserved with Prolong Gold with DAPI (Invitrogen, cat. # P36931). Colocalization analysis was performed with Leica Application Suite X (LAS X).

Bacterial Culture

Single colony of *C. acnes* was inoculated into 5 mL of Reinforced Clostridial Media (RCM) (Thermofisher, cat. # CM0149B) and cultured at 37°C under anaerobic conditions until early logarithmic growth phase ($OD_{600} = 0.1 - 0.3$). Bacteria pellets were harvested by centrifugation at 5,000xg for 10 minutes and washed with 1 X PBS three times.

Axenic Culture Assay

C. acnes were cultured and harvested as described above. 5×10^7 bacteria were resuspended in RCM prior to oxygen and nitrogen donor exposure. After two-hour incubation at 37°C with H_2O_2 (Sigma 386790), TBHP (Sigma 458139), and DETA NONOate (Cayman, cat

#146724–94-9) at various concentrations, bacteria were serially diluted in fresh RCM, and dilutions were plated onto Brucella agar plates with 5% Sheep Blood (Fisher, cat. # R01255). CFU (colony forming unit) were counted after 7 days of incubation at 37°C using Anaeropack (Fisher, cat. # 23–246-376). The two-hour incubation time was chosen according to Ramsey et al *PLoS Pathog.* **13**, e1006225 (2017).

Phagocytosis Assay

In vitro macrophages were generated as described above with LPS (100ng/mL) (Enzo, cat. # ALX-581–007-L001) + IFN-γ (20ng/mL) (BD, cat. # 554617) for 1 day or M-CSF (50 ng/ml) (R&D Systems, cat. # 216MC025/CF), IL-4 (20ng/mL) (Peprotech, cat. # 200–04) and squalene (1 mM) (Sigma, cat. # S3626–100ML) for 2 days at concentration of 500,000 macrophages per well in 24-well plate. Cytokine and squalene-treated macrophages were washed three times with PBS. *C. acnes* were labeled using PKH26 general cell membrane labeling kit (Sigma, cat. # MIDI26–1KT) according to manufacturer's protocol. Macrophages were incubated with either PKH26-labelled *C. acnes* at MOI 10 or latex beads (Sigma, cat. # L2778–1mL) for 24 hours. Cells were prepared with cold PBS washing and extracellular bacteria were killed with 300 μg/mL gentamicin (Life technologies, cat. # 15710–064). Cells were then acquired with LSR II flow cytometer (BD) and analyzed with FlowJo (BD) for geometric mean fluorescence intensity (MFI).

Antimicrobial Assays

Macrophages were incubated with bacteria at MOI 10 for 1 hour and 24 hour at 37°C. Cells were washed 3 times with cold PBS. Extracellular bacteria were killed with 300 μg/mL gentamicin (Life technologies, cat. # 15710–064). Cells were lysed with a 10-minute treatment with 0.5% saponin (Sigma, cat. # 47036–50G-F). A dilution series was plated on Brucella agar plates with 5% Sheep Blood (Fisher, cat. # R01255) to determine viable intracellular bacteria by CFU counting after 7 days of incubation at 37°C using Anaeropack (Fisher, cat. # 23–246-376). Antimicrobial activity was calculated by subtracting the 24-hour CFU count from the 1-hour CFU count and divided by the 1-hour CFU count to determine the percentage of killing.

ELISA

After 24 hours of stimulation with *C. acnes*, cell culture supernatant was extracted to be used immediately or stored at −20°C. Total IL-18 (R&D Systems, cat. # DY318–05) release was measured by ELISA according to the manufacturer's protocol.

Statistical Analysis.

Statistical analyses were calculated using GraphPad Prism version 8.0, and p values 0.05 were assigned as significant. For comparisons involving two groups, an unpaired Student t test with two-tailed p-value analysis was performed, unless otherwise stated in the figure legend.

Supplementary Material

Refer to Web version on PubMed Central for supplementary material.

Acknowledgements:

Data and materials availability:

The scRNA-seq acne lesion data of this study have been deposited in the database Gene Expression Omnibus (GEO) under accession no. GSE175817. The scRNA-seq in vitro macrophage data are available under accession no. GSE193973. The spatial sequencing data are available at the GEO under accession no. GSE175856. The Seq-Scope data are available at the GEO under accession no. GSE186601. The re-analysis of the myeloid cluster from the scRNA-seq data derived from a variety of skin inflammatory skin diseases was previously published and deposited under accession no. GSE150672.

References and Notes:

1. Hay RJ et al. , The global burden of skin disease in 2010: an analysis of the prevalence and impact of skin conditions. J. Invest. Dermatol 134, 1527–1534 (2014). [PubMed: 24166134]

2. Fried RG, Acne vulgaris: The psychosocial and psychological burden of llness. The Dermatologist 21, 28–32 (2013).

3. Zaraa I et al. , Severity of acne and its impact on quality of life. Skinmed 11, 148–153 (2013). [PubMed: 23930353]

4. Mooney T, Preventing psychological distress in patients with acne. Nurs. Stand 28, 42–48 (2014).

5. Aktan S, Ozmen E, Sanli B, Anxiety, depression, and nature of acne vulgaris in adolescents. Int. J. Dermatol 39, 354–357 (2000). [PubMed: 10849125]

6. Halvorsen JA, Dalgard F, Thoresen M, Bjertness E, Lien L, Is the association between acne and mental distress influenced by diet? Results from a cross-sectional population study among 3775 late adolescents in Oslo, Norway. BMC Public Health 9, 340 (2009). [PubMed: 19758425]

7. Purvis D, Robinson E, Merry S, Watson P, Acne, anxiety, depression and suicide in teenagers: A cross-sectional survey of New Zealand secondary school students. Journal of paediatrics and child health 42, 793–796 (2006). [PubMed: 17096715]

8. Kilkenny M et al. , Acne in Victorian adolescents: associations with age, gender, puberty and psychiatric symptoms. J. Paediatr. Child Health 33, 430–433 (1997). [PubMed: 9401889]

9. Walker N, Lewis-Jones MS, Quality of life and acne in Scottish adolescent schoolchildren: use of the Children's Dermatology Life Quality Index (CDLQI) and the Cardiff Acne Disability Index (CADI). J. Eur. Acad. Dermatol. Venereol 20, 45–50 (2006). [PubMed: 16405607]

10. Tasoula E et al. , The impact of acne vulgaris on quality of life and psychic health in young adolescents in Greece. Results of a population survey. An. Bras. Dermatol 87, 862–869 (2012). [PubMed: 23197205]

11. Picardi A, Mazzotti E, Pasquini P, Prevalence and correlates of suicidal ideation among patients with skin disease. J. Am. Acad. Dermatol 54, 420–426 (2006). [PubMed: 16488292]

12. Leyden JJ, New understandings of the pathogenesis of acne. Journal of the American Academy of Dermatology 32, S15–S25 (1995). [PubMed: 7738222]

13. Lovászi M et al. , Sebum lipids influence macrophage polarization and activation. British Journal of Dermatology 177, 1671–1682 (2017). [PubMed: 28646583]

14. Smith K, Thiboutot D, Thematic review series: skin lipids. Sebaceous gland lipids: friend or foe? Journal of lipid research 49, 271–281 (2008). [PubMed: 17975220]

15. Zouboulis C, Jourdan E, Picardo M, Acne is an inflammatory disease and alterations of sebum composition initiate acne lesions. Journal of the European Academy of Dermatology and Venereology 28, 527–532 (2014). [PubMed: 24134468]

16. Byrd AL, Belkaid Y, Segre JA, The human skin microbiome. Nature Reviews Microbiology 16, 143 (2018). [PubMed: 29332945]

17. Gribbon E, Cunliffe W, Holland K, Interaction of Propionibacterium acnes with skin lipids in vitro. Microbiology 139, 1745–1751 (1993).

18. Pappas A, Johnsen S, Liu J-C, Eisinger M, Sebum analysis of individuals with and without acne. Dermatoendocrinol. 1, 157–161 (2009). [PubMed: 20436883]

19. Rosignoli C, Nicolas J, Jomard A, Michel S, Involvement of the SREBP pathway in the mode of action of androgens in sebaceous glands in vivo. Experimental dermatology 12, 480–489 (2003). [PubMed: 12930306]

20. Ottaviani M et al. , Peroxidated squalene induces the production of inflammatory mediators in HaCaT keratinocytes: a possible role in acne vulgaris. Journal of investigative dermatology 126, 2430–2437 (2006). [PubMed: 16778793]

21. De Jong A et al. , CD1a-autoreactive T cells recognize natural skin oils that function as headless antigens. Nature immunology 15, 177 (2014). [PubMed: 24362891]

22. Saint-Leger D, Bague A, Lefebvre E, Cohen E, Chivot M, A possible role for squalene in the pathogenesis of acne. II. In vivo study of squalene oxides in skin surface and intra-comedonal lipids of acne patients. Br. J. Dermatol 114, 543–552 (1986). [PubMed: 2941050]

23. MILLS OH, PORTE M, KLIGMAN AM, Enhancement of comedogenic substances by ultraviolet radiation. British Journal of Dermatology 98, 145–150 (1978). [PubMed: 147099]

24. O'Hagan DT, Ott GS, Nest GV, Rappuoli R, Giudice GD, The history of MF59® adjuvant: a phoenix that arose from the ashes. Expert review of vaccines 12, 13–30 (2013). [PubMed: 23256736]

25. Jiang H, Li C, Common Pathogenesis of Acne Vulgaris and Atherosclerosis. Inflammation 42, 1–5 (2018).

26. Siegel-Axel D, Daub K, Seizer P, Lindemann S, Gawaz M, Platelet lipoprotein interplay: trigger of foam cell formation and driver of atherosclerosis. Cardiovasc. Res 78, 8–17 (2008). [PubMed: 18218686]

27. Willemsen L, de Winther MP, Macrophage subsets in atherosclerosis as defined by single-cell technologies. The Journal of pathology 250, 705–714 (2020). [PubMed: 32003464]

28. Cao F, Castrillo A, Tontonoz P, Re F, Byrne GI, Chlamydia pneumoniae-induced macrophage foam cell formation is mediated by Toll-like receptor 2. Infect. Immun 75, 753–759 (2007). [PubMed: 17145941]

29. Portugal LR et al. , Influence of low-density lipoprotein (LDL) receptor on lipid composition, inflammation and parasitism during Toxoplasma gondii infection. Microbes and Infection 10, 276–284 (2008). [PubMed: 18316222]

30. Russell DG, Cardona P-J, Kim M-J, Allain S, Altare F, Foamy macrophages and the progression of the human tuberculosis granuloma. Nature immunology 10, 943–948 (2009). [PubMed: 19692995]

31. Tedgui A, Mallat Z, Cytokines in atherosclerosis: pathogenic and regulatory pathways. Physiological reviews 86, 515–581 (2006). [PubMed: 16601268]

32. Trivedi NR, Gilliland KL, Zhao W, Liu W, Thiboutot DM, Gene array expression profiling in acne lesions reveals marked upregulation of genes involved in inflammation and matrix remodeling. J Invest Dermatol 126, 1071–1079 (2006). [PubMed: 16528362]

33. Kelhala HL et al. , IL-17/Th17 pathway is activated in acne lesions. PLoS One 9, e105238 (2014). [PubMed: 25153527]

34. Butler A, Hoffman P, Smibert P, Papalexi E, Satija R, Integrating single-cell transcriptomic data across different conditions, technologies, and species. Nature biotechnology 36, 411–420 (2018).

35. Rizvi AH et al. , Single-cell topological RNA-seq analysis reveals insights into cellular differentiation and development. Nat. Biotechnol 35, 551–560 (2017). [PubMed: 28459448]

36. Seumois G, Vijayanand P, Single-cell analysis to understand the diversity of immune cell types that drive disease pathogenesis. J. Allergy Clin. Immunol 144, 1150–1153 (2019). [PubMed: 31703762]

37. Szabo PA et al. , Single-cell transcriptomics of human T cells reveals tissue and activation signatures in health and disease. Nature communications 10, 4706 (2019).

38. Young MD, Behjati S, SoupX removes ambient RNA contamination from droplet-based single-cell RNA sequencing data. Gigascience 9, giaa151 (2020). [PubMed: 33367645]

39. Stuart T et al. , Comprehensive Integration of Single-Cell Data. Cell 177, 1888–1902 e1821 (2019). [PubMed: 31178118]

40. Agak GW et al. , Propionibacterium acnes Induces an IL-17 Response in Acne Vulgaris that Is Regulated by Vitamin A and Vitamin D. J. Invest. Dermatol 134, 366–373 (2014). [PubMed: 23924903]

41. Kim J et al. , Activation of toll-like receptor 2 in acne triggers inflammatory cytokine responses. J. Immunol 169, 1535–1541 (2002). [PubMed: 12133981]

42. Kistowska M et al. , IL-1beta drives inflammatory responses to propionibacterium acnes in vitro and in vivo. J. Invest. Dermatol 134, 677–685 (2014). [PubMed: 24157462]

43. Gordon S, Alternative activation of macrophages. Nature reviews immunology 3, 23–35 (2003).

44. Gerrick KY et al. , Transcriptional profiling identifies novel regulators of macrophage polarization. PLoS One 13, (2018).

45. Guo MM-H, Chang L-S, Huang Y-H, Wang F-S, Kuo H-C, Epigenetic Regulation of Macrophage Marker Expression Profiles in Kawasaki Disease. Frontiers in Pediatrics 8, (2020).

46. Martinez FO, Gordon S, Locati M, Mantovani A, Transcriptional profiling of the human monocyte-to-macrophage differentiation and polarization: new molecules and patterns of gene expression. The Journal of Immunology 177, 7303–7311 (2006). [PubMed: 17082649]

47. Cochain C et al. , Single-Cell RNA-Seq Reveals the Transcriptional Landscape and Heterogeneity of Aortic Macrophages in Murine Atherosclerosis. Circ. Res 122, 1661–1674 (2018). [PubMed: 29545365]

48. Jaitin DA et al. , Lipid-Associated Macrophages Control Metabolic Homeostasis in a Trem2-Dependent Manner. Cell 178, 686–698 e614 (2019). [PubMed: 31257031]

49. Keren-Shaul H et al. , A Unique Microglia Type Associated with Restricting Development of Alzheimer's Disease. Cell 169, 1276–1290 e1217 (2017). [PubMed: 28602351]

50. Lavin Y et al. , Innate Immune Landscape in Early Lung Adenocarcinoma by Paired Single-Cell Analyses. Cell 169, 750–765 e717 (2017). [PubMed: 28475900]

51. Xiong X et al. , Landscape of Intercellular Crosstalk in Healthy and NASH Liver Revealed by Single-Cell Secretome Gene Analysis. Mol. Cell 75, 644–660 e645 (2019). [PubMed: 31398325]

52. Wang EC, Dai Z, Ferrante AW, Drake CG, Christiano AM, A subset of TREM2+ dermal macrophages secretes oncostatin m to maintain hair follicle stem cell quiescence and inhibit hair growth. Cell Stem Cell 24, 654–669. e656 (2019). [PubMed: 30930146]

53. Xue D, Tabib T, Morse C, Lafyatis R, Transcriptome landscape of myeloid cells in human skin reveals diversity, rare populations and putative DC progenitors. Journal of dermatological science 97, 41–49 (2020). [PubMed: 31836271]

54. Casanova-Acebes M et al. , Tissue-resident macrophages provide a pro-tumorigenic niche to early NSCLC cells. Nature, 1–7 (2021).

55. Hughes TK et al. , Second-strand synthesis-based massively parallel scRNA-Seq reveals cellular states and molecular features of human inflammatory skin pathologies. Immunity 53, 878–894. e877 (2020). [PubMed: 33053333]

56. He H et al. , Single-cell transcriptome analysis of human skin identifies novel fibroblast subpopulation and enrichment of immune subsets in atopic dermatitis. Journal of Allergy and Clinical Immunology 145, 1615–1628 (2020). [PubMed: 32035984]

57. Liu J et al. , Single-cell RNA sequencing of psoriatic skin identifies pathogenic Tc17 cell subsets and reveals distinctions between CD8+ T cells in autoimmunity and cancer. Journal of Allergy and Clinical Immunology 147, 2370–2380 (2021). [PubMed: 33309739]

58. Kim J et al. , Single-cell transcriptomics applied to emigrating cells from psoriasis elucidate pathogenic versus regulatory immune cell subsets. Journal of Allergy and Clinical Immunology, (2021).

59. Zhang X, Yin M, Zhang L.-j., Keratin 6, 16 and 17—Critical Barrier Alarmin Molecules in Skin Wounds and Psoriasis. Cells 8, 807 (2019).

60. Fuchs E, Raghavan S, Getting under the skin of epidermal morphogenesis. Nature Reviews Genetics 3, 199–209 (2002).

61. Gerber PA et al. , Systematic identification and characterization of novel human skin-associated genes encoding membrane and secreted proteins. PloS one 8, e63949 (2013). [PubMed: 23840300]

62. Suo L et al. , Dietary vitamin A impacts refractory telogen. Frontiers in cell and developmental biology 9, 129 (2021).

63. Kang S et al. , Inflammation and extracellular matrix degradation mediated by activated transcription factors nuclear factor-κB and activator protein-1 in inflammatory acne lesions in vivo. The American journal of pathology 166, 1691–1699 (2005). [PubMed: 15920154]

64. Sissaoui S et al. , Genomic Characterization of Endothelial Enhancers Reveals a Multifunctional Role for NR2F2 in Regulation of Arteriovenous Gene Expression. Circ. Res, (2020).

65. Chenivesse C, Tsicopoulos A, CCL18 - Beyond chemotaxis. Cytokine 109, 52–56 (2018). [PubMed: 29402725]

66. Ma F et al. , The cellular architecture of the antimicrobial response network in human leprosy granulomas. Nature immunology 22, 839–850 (2021). [PubMed: 34168371]

67. Gao Y et al. , Single cell transcriptional zonation of human psoriasis skin identifies an alternative immunoregulatory axis conducted by skin resident cells. Cell death & disease 12, 1–13 (2021). [PubMed: 33414393]

68. Rojahn TB et al. , Single-cell transcriptomics combined with interstitial fluid proteomics defines cell type–specific immune regulation in atopic dermatitis. Journal of Allergy and Clinical Immunology 146, 1056–1069 (2020). [PubMed: 32344053]

69. Eraslan G et al. , Single-nucleus cross-tissue molecular reference maps to decipher disease gene function. bioRxiv, (2021).

70. Huang D et al. , Targeting regulator of G protein signaling 1 in tumor-specific T cells enhances their trafficking to breast cancer. Nature Immunology, 1–15 (2021). [PubMed: 33335328]

71. Wu B et al. , Mitochondrial aspartate regulates TNF biogenesis and autoimmune tissue inflammation. Nature immunology 22, 1551–1562 (2021). [PubMed: 34811544]

72. Manich G et al. , Differential roles of TREM2+ microglia in anterograde and retrograde axonal injury models. Frontiers in Cellular Neuroscience 14, 369 (2020).

73. Soto I et al. , Meox2 haploinsufficiency increases neuronal cell loss in a mouse model of Alzheimer's disease. Neurobiology of aging 42, 50–60 (2016). [PubMed: 27143421]

74. Raha-Chowdhury R et al. , Erythromyeloid-derived TREM2: a major determinant of Alzheimer's disease pathology in down syndrome. Journal of Alzheimer's Disease 61, 1143–1162 (2018).

75. Lopez D et al. , SaVanT: a web-based tool for the sample-level visualization of molecular signatures in gene expression profiles. BMC genomics 18, 824 (2017). [PubMed: 29070035]

76. Griffith JW, Sokol CL, Luster AD, Chemokines and chemokine receptors: positioning cells for host defense and immunity. Annu. Rev. Immunol 32, 659–702 (2014). [PubMed: 24655300]

77. Bergen V, Lange M, Peidli S, Wolf FA, Theis FJ, Generalizing RNA velocity to transient cell states through dynamical modeling. Nature biotechnology 38, 1408–1414 (2020).

78. La Manno G et al. , RNA velocity of single cells. Nature 560, 494–498 (2018). [PubMed: 30089906]

79. Peters JM, Blainey PC, Bryson BD, Consensus transcriptional states describe human mononuclear phagocyte diversity in the lung across health and disease. bioRxiv, (2020).

80. Ershov P et al. , Enzymes in the Cholesterol Synthesis Pathway: Interactomics in the Cancer Context. Biomedicines 9, 895 (2021). [PubMed: 34440098]

81. Peck B, Schulze A, Lipid desaturation–the next step in targeting lipogenesis in cancer? The FEBS journal 283, 2767–2778 (2016). [PubMed: 26881388]

82. Turkish AR et al. , Identification of Two Novel Human Acyl-CoA Wax Alcohol Acyltransferases MEMBERS OF THE DIACYLGLYCEROL ACYLTRANSFERASE 2 (DGAT2) GENE SUPERFAMILY. J. Biol. Chem 280, 14755–14764 (2005). [PubMed: 15671038]

83. Chitraju C, Walther TC, Farese RV, The triglyceride synthesis enzymes DGAT1 and DGAT2 have distinct and overlapping functions in adipocytes. J. Lipid Res 60, 1112–1120 (2019). [PubMed: 30936184]

84. Moncada R et al. , Integrating microarray-based spatial transcriptomics and single-cell RNA-seq reveals tissue architecture in pancreatic ductal adenocarcinomas. Nature biotechnology 38, 333–342 (2020).

85. Cho C-S et al. , Microscopic examination of spatial transcriptome using Seq-Scope. Cell, (2021).

86. Negi M et al. , Localization of Propionibacterium acnes in granulomas supports a possible etiologic link between sarcoidosis and the bacterium. Modern Pathology 25, 1284–1297 (2012). [PubMed: 22596102]

87. Turnbull IR et al. , Cutting edge: TREM-2 attenuates macrophage activation. J. Immunol 177, 3520–3524 (2006). [PubMed: 16951310]

88. Mantovani A et al. , The chemokine system in diverse forms of macrophage activation and polarization. Trends in immunology 25, 677–686 (2004). [PubMed: 15530839]

89. Liu PT et al. , CD209+ macrophages mediate host defense against Propionibacterium acnes. The Journal of Immunology 180, 4919–4923 (2008). [PubMed: 18354216]

90. Kohno Y et al. , Kinetic study of quenching reaction of singlet oxygen and scavenging reaction of free radical by squalene in n-butanol. Biochimica et Biophysica Acta (BBA)-Lipids and Lipid Metabolism 1256, 52–56 (1995). [PubMed: 7742356]

91. Fernando IPS et al. , Squalene isolated from marine macroalgae Caulerpa racemosa and its potent antioxidant and anti-inflammatory activities. J. Food Biochem 42, e12628 (2018).

92. Levin R, Grinstein S, Canton J, The life cycle of phagosomes: formation, maturation, and resolution. Immunological reviews 273, 156–179 (2016). [PubMed: 27558334]

93. Santabárbara-Ruiz P et al. , ROS-induced JNK and p38 signaling is required for unpaired cytokine activation during Drosophila regeneration. PLoS Genet 11, e1005595 (2015). [PubMed: 26496642]

94. Hien HTM, Ha NC, Hong DD, Squalene promotes cholesterol homeostasis in macrophage and hepatocyte cells via activation of liver X receptor (LXR) α and β. Biotechnology letters 39, 1101–1107 (2017). [PubMed: 28492976]

95. Nugent AA et al. , TREM2 regulates microglial cholesterol metabolism upon chronic phagocytic challenge. Neuron 105, 837–854. e839 (2020). [PubMed: 31902528]

96. Seidman JS et al. , Niche-Specific Reprogramming of Epigenetic Landscapes Drives Myeloid Cell Diversity in Nonalcoholic Steatohepatitis. Immunity, (2020).

97. Chapman AC, VIII.—Spinacene: a new hydrocarbon from certain fish liver oils. Journal of the Chemical Society, Transactions 111, 56–69 (1917).

98. Chapman AC, XC.—Spinacene: its oxidation and decomposition. Journal of the Chemical Society, Transactions 123, 769–779 (1923).

99. Tör csik D et al. , Genome wide analysis of TLR1/2-and TLR4-activated SZ95 sebocytes reveals a complex immune-competence and identifies serum amyloid A as a marker for activated sebaceous glands. PloS one 13, e0198323 (2018). [PubMed: 29927962]

100. Papakonstantinou E et al. , Matrix metalloproteinases of epithelial origin in facial sebum of patients with acne and their regulation by isotretinoin. J. Invest. Dermatol 125, 673–684 (2005). [PubMed: 16185265]

101. Schönbeck U, Mach F, Libby P, Generation of biologically active IL-1β by matrix metalloproteinases: a novel caspase-1-independent pathway of IL-1β processing. The Journal of Immunology 161, 3340–3346 (1998). [PubMed: 9759850]

102. Dinarello C, Novick D, Kim S, Kaplanski G, Interleukin-18 and IL-18 binding protein. Frontiers in immunology 4, 289 (2013). [PubMed: 24115947]

103. Kannan Y et al. , IkappaBzeta augments IL-12- and IL-18-mediated IFN-gamma production in human NK cells. Blood 117, 2855–2863 (2011). [PubMed: 21224476]

104. Smeltz RB, Profound Enhancement of the IL-12/IL-18 Pathway of IFN-γ Secretion in Human CD8+ Memory T Cell Subsets via IL-15. The Journal of Immunology 178, 4786–4792 (2007). [PubMed: 17404259]

105. Heiseke AF et al. , CCL17 Promotes Intestinal Inflammation in Mice and Counteracts Regulatory T Cell–Mediated Protection From Colitis. Gastroenterology 142, 335–345 (2012). [PubMed: 22057112]

106. Weber C et al. , CCL17-expressing dendritic cells drive atherosclerosis by restraining regulatory T cell homeostasis in mice. The Journal of clinical investigation 121, 2898–2910 (2011). [PubMed: 21633167]

107. Weber GF et al. , Phosphorylation-dependent interaction of osteopontin with its receptors regulates macrophage migration and activation. J. Leukoc. Biol 72, 752–761 (2002). [PubMed: 12377945]

108. Mazière C, Gomila C, Mazière J-C, Oxidized low-density lipoprotein increases osteopontin expression by generation of oxidative stress. Free Radical Biology and Medicine 48, 1382–1387 (2010). [PubMed: 20211246]

109. Tohyama M et al. , CXCL16 is a novel mediator of the innate immunity of epidermal keratinocytes. Int. Immunol 19, 1095–1102 (2007). [PubMed: 17855433]

110. Katzenelenbogen Y et al. , Coupled scRNA-seq and intracellular protein activity reveal an immunosuppressive role of TREM2 in cancer. Cell 182, 872–885. e819 (2020). [PubMed: 32783915]

111. Yu HJ et al. , Steroid acne vs. Pityrosporumfolliculitis: the incidence ofPityrosporum ovaleand the effect of antifungal drugs in steroid acne. Int. J. Dermatol 37, 772–777 (1998). [PubMed: 9802688]

112. Ahmadvand A et al. , Evaluating the effects of oral and topical simvastatin in the treatment of acne vulgaris: a double-blind, randomized, placebo-controlled clinical trial. Current clinical pharmacology 13, 279–283 (2018). [PubMed: 30129417]

113. Trapnell C et al. , The dynamics and regulators of cell fate decisions are revealed by pseudotemporal ordering of single cells. Nature biotechnology 32, 381–386 (2014).

114. Chen EY et al. , Enrichr: interactive and collaborative HTML5 gene list enrichment analysis tool. BMC bioinformatics 14, 128 (2013). [PubMed: 23586463]

115. Kuleshov MV et al. , Enrichr: a comprehensive gene set enrichment analysis web server 2016 update. Nucleic acids research 44, W90–W97 (2016). [PubMed: 27141961]

116. Bindea G et al. , ClueGO: a Cytoscape plug-in to decipher functionally grouped gene ontology and pathway annotation networks. Bioinformatics 25, 1091–1093 (2009). [PubMed: 19237447]
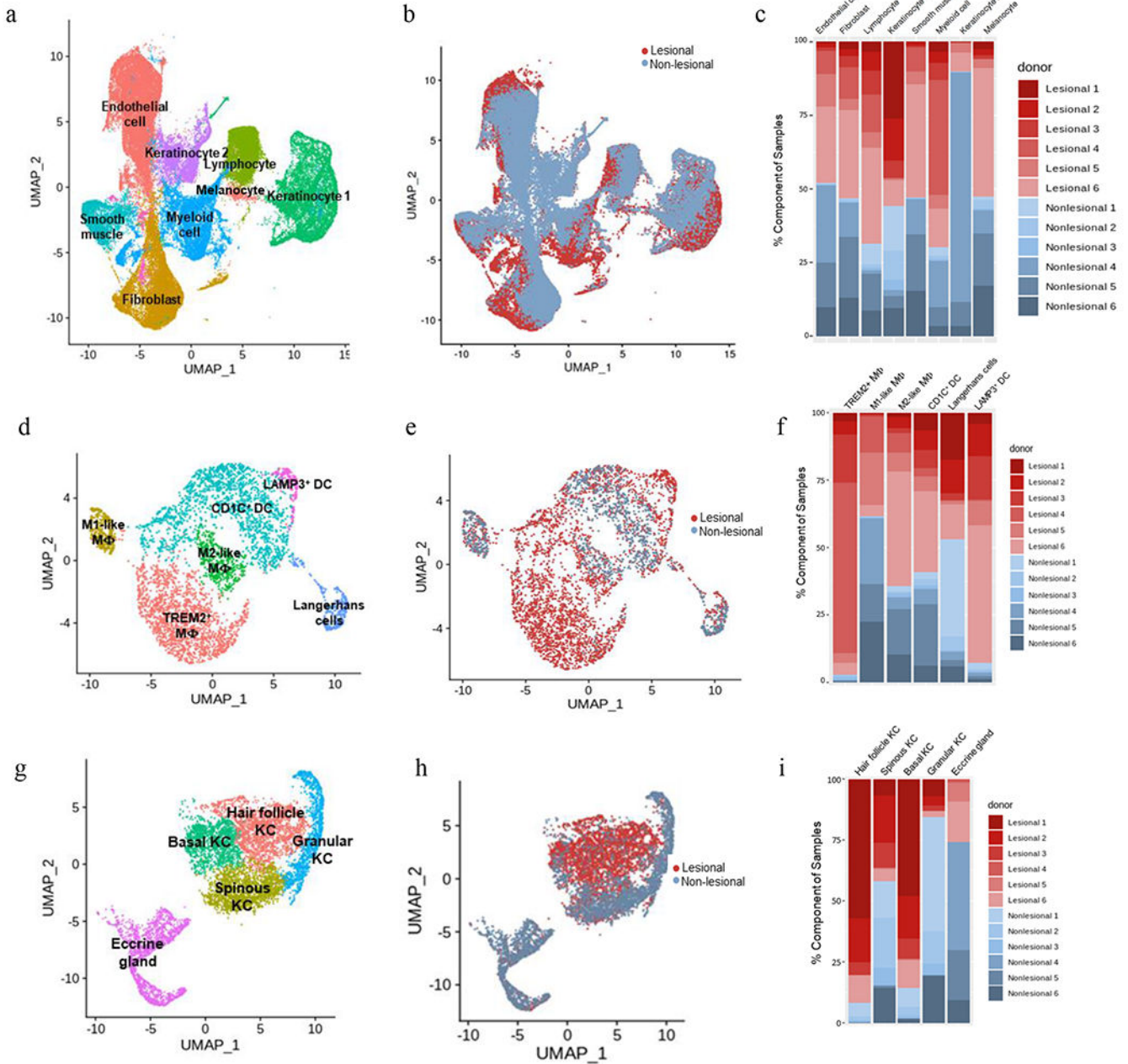
Author Manuscript

Author Manuscript

Author Manuscript

Author Manuscript

Fig. 1. Cell Types Recovered in Lesional and Non-lesional Acne

a. UMAP plot for 62,168 cells from acne patients colored by cell type.

b. UMAP plot for 62,168 cells colored by lesional types with 32,966 cells from lesional skin and 29,202 cells from non-lesional skin. Lesional cells are shown in red while non-lesional cells are shown in blue.

c. Stacked bar-plot showing the donor and lesion type composition for each of the cell types. Lesional cells are shown in red while non-lesional cells are shown in blue.

d. UMAP plot for 4,370 myeloid cells from acne patients colored by cell types.

e. UMAP plot for 4,370 myeloid cells colored by lesional types with 3,152 myeloid cells from lesional skin and 1,218 myeloid cells from non-lesional skin. Lesional cells are shown in red while non-lesional cells are shown in blue.

f. Stacked bar-plot showing the donor and lesion type composition for each of the cell types. Lesional cells are shown in red while non-lesional cells are shown in blue.

g. UMAP plot for 8,271 KCs from acne patients colored by cell types.

h. UMAP plot for 8,271 keratinocytes colored by lesional types with 4,473 keratinocytes from lesional skin and 3,798 keratinocytes from non-lesional skin. Lesional cells are shown in red while non-lesional cells are shown in blue.

i. Stacked bar-plot showing the donor and lesion type composition for each of the cell types. Lesional cells are shown in red while non-lesional cells are shown in blue.
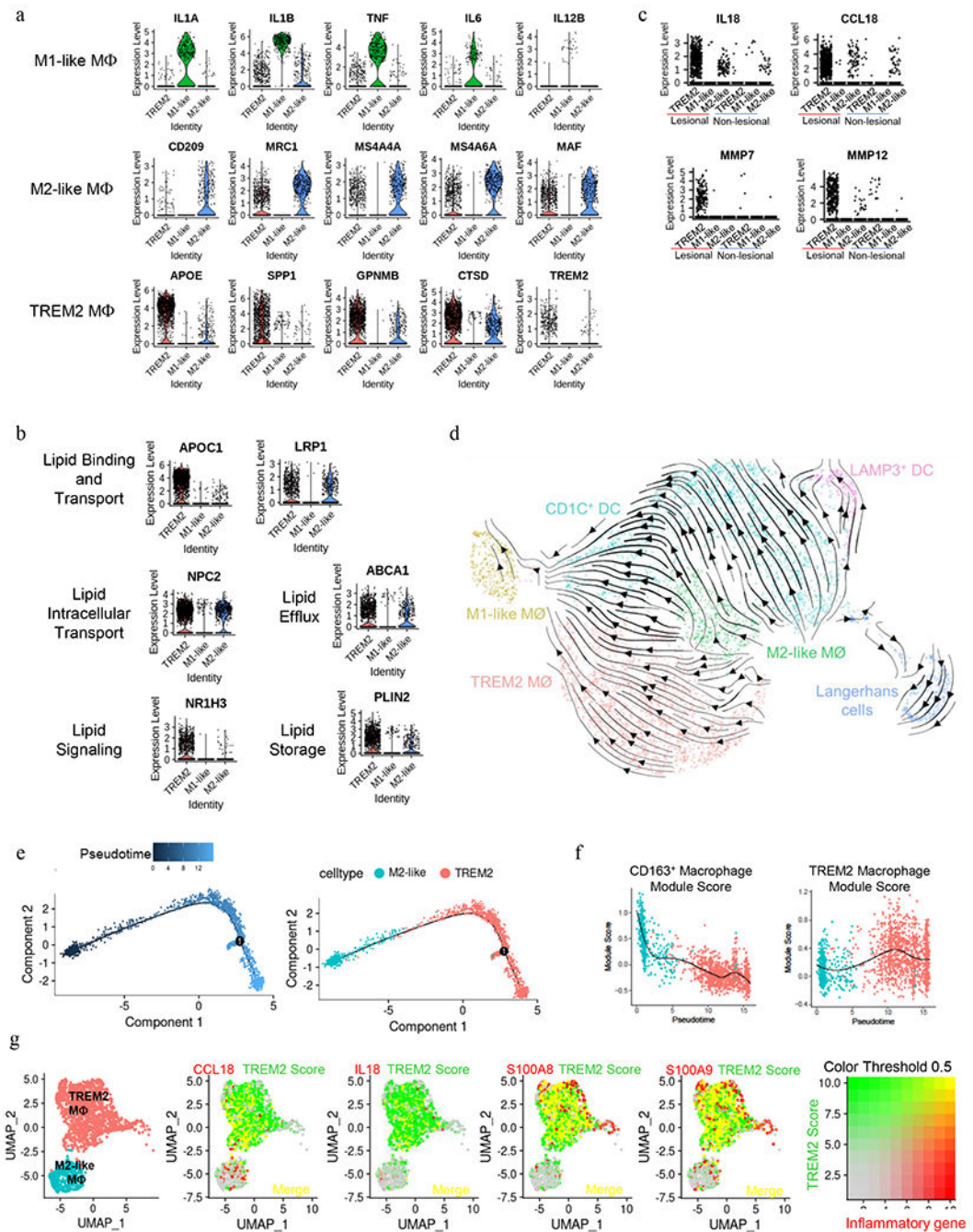
Fig. 2. Characterization of TREM2 Macrophages

a. Violin plots showing the normalized expression levels for genes in macrophage sub-clusters.

b. Violin plots showing normalized expression of categories of lipid processing genes based on gene ontology categories.

c. Jitter plots showing normalized expression of macrophage sub-clusters separated by lesional versus non-lesional cells.

d. Velocity field projected onto the UMAP plot of myeloid cells using the velocity_embedding_stream function. All scVelo functions were used with default parameters. Cells colored based on cell type as represented in Fig. 1d.

e. Pseudotime trajectory generated by Monocle2 of TREM2 and M2-like macrophage subcluster. (Left) A total of 1,975 cells were imported from Seurat data are colored according to the pseudotime dark blue to light blue. (Right) Trajectory showing the distribution of cells colored based on cell type.

f. Scatter plot showing the correlation between TREM2 and M2-like macrophage pseudotimes and module scores calculated using transcriptional profiles from CD163+ Macrophage and TREM2 Macrophage as described in Peters, J.M. et. al *bioRxiv* scRNA-seq studies of lung. The color of the dots represents the subcluster identity of the cells.

g. (Far Left) UMAP plot for 1,975 cells of TREM2 and M2-like macrophage. (Right) Co-expression of inflammatory genes *(CCL18, IL18, S100A8, S100A9)* in red and TREM2 score (*APOE, CTSB, TREM2, CD68, GPNMB, LPL, SPP1, LGALS3, TYROBP)* via AddModuleScore function in Seurat in green with co-expression in yellow via Seurat FeaturePlot function with blend=T and blend.threshold = 0.5.
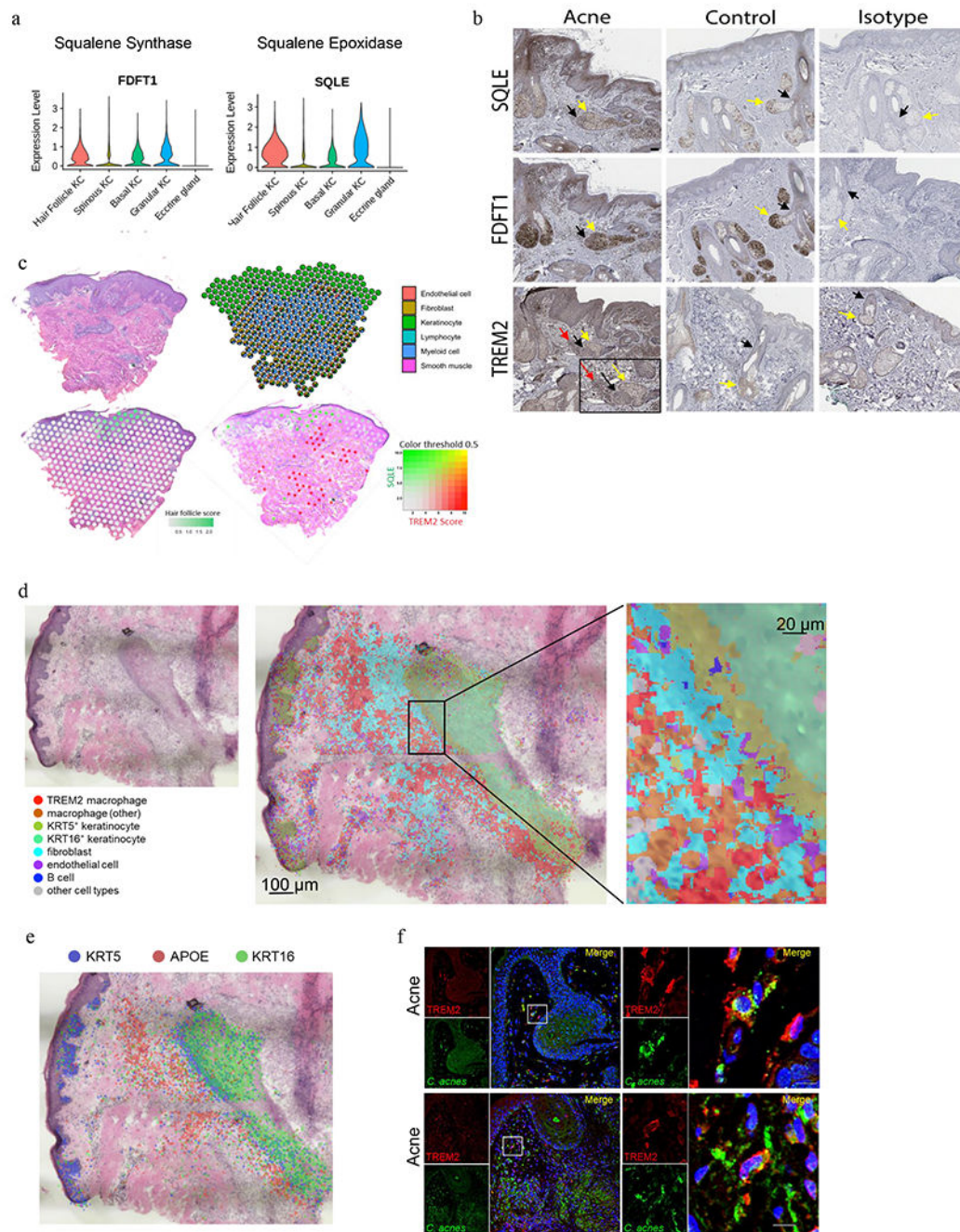
Fig. 3. KCs in the hair follicles present in acne lesions is capable of squalene synthesis

a. Violin plots showing the normalized expression levels of FDFT1 (squalene synthase) and SQLE (squalene epoxidase) for keratinocyte sub-clusters.

b. Representative immunohistochemistry staining of FDFT1, SQLE, TREM2 encoded protein (n=3) showing hair follicle (black arrow), sebocytes (yellow arrow), and TREM2+ cells (red arrow). Acne skin samples were obtained from papules of acne patients and controls were from healthy skin on the scalp. Scale bar = 100 μm.

c. (Top Left) H & E staining of the acne biopsy used for spatial sequencing. (Top Right) Scatter pie plot showing the cell type composition of the acne spatial-seq sample. Each spot is represented as a pie chart showing the relative proportion of the cell types. (Bottom Left) Spatial plot showing the expression of hair follicle score, which is the sum of *KRT6C, KRT6B, KRT17* expression. (Bottom Right) Spatial plot showing the expression of *SQLE* and TREM2 score, which is the sum of *APOE, CTSB, TREM2, CD68, GPNMB, LPL, SPP1, LGALS3, TYROBP* expression.

d. (Left) H&E staining of the acne biopsy used for Seq-Scope analysis. (Middle) Spatial plot used to visualize cell types clusters of 5mm-sided square grids with an average of 145 genes and 167 transcripts across 3,558 grids in an acne lesion. (Right) Boxed region showing the magnified spatial plot with 1um intervals between grids.

e. Spatial plot showing overlay of *KRT5* in blue, *APOE* in red, and *KRT16* in green with 2um intervals between grids.

f. Representative immunofluorescence staining in lesional acne skin biopsy samples for expression of TREM2 in red, *C. acnes* in green, and colocalization in yellow (n=4 acne, n=2 normal skin). Scale bar = 20 μm.
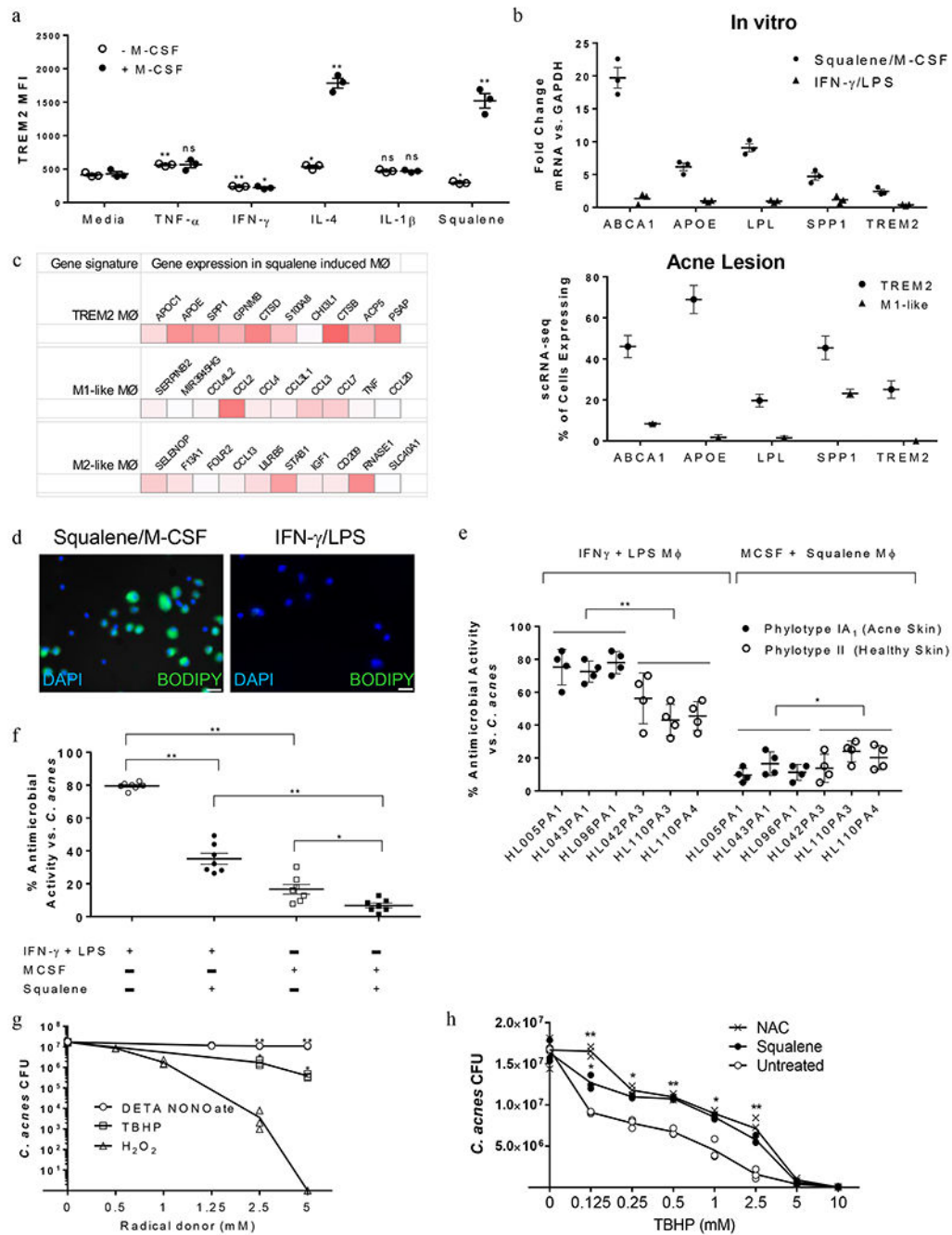
Fig. 4. Squalene Induce TREM2 Expression in Macrophages in vitro and blocks oxidative killing of *C. acnes*.

a. Geometric mean fluorescence intensity (MFI) of TREM2 expression with the different stimuli with and without M-CSF (n=3). Results are shown as mean ± SEM. P-values were calculated using unpaired Student's t-test of the cytokine-treated sample compared to the media sample (with or without MCSF). ns = not significant, * = p-value < 0.05, ** = p-value < 0.01.

b. (Top) Real-time PCR of fold change of relative gene expression to GAPDH on in vitro macrophages (n=3). Results are shown as mean ± SEM. (Bottom) scRNA-seq average

percent of cell expressing lipid genes for donor with more than 10 cells expressing the marker genes in acne lesion. Results are shown as mean ± SEM.

c. Gene expression of the top 10 signature genes for TREM2 macrophages, M1-like macrophages and M2-like macrophages from acne lesions in all cells from the in vitro derived macrophages.

d. Immunocytochemical staining of in vitro stimulated macrophages. DAPI is in blue and BODIPY is in green. Scale bar = 20 μm.

e. Macrophages were stimulated with IFN-γ + LPS with and without squalene for 24 hours or MCSF with and without squalene for 48 hours. Macrophages were then activated with different *C. acnes* strains for 24 hours. Antimicrobial activity was calculated by subtracting 24-hour CFU (colony counting unit) count with 1-hour CFU count and divide by CFU at 24-hour to determine the percentage of killing of each *C. acnes* strain. Results are shown as mean ± SEM. P-values were calculated using unpaired Student's t-test of the antimicrobial activity against phylotype IA_1 *C. acnes* strains compared to the antimicrobial activity against phylotype II *C. acnes* strains. * = p-value < 0.05, ** = p-value < 0.01.

f. Macrophages were stimulated with IFN-γ + LPS with and without squalene for 24 hours or MCSF with and without squalene for 48 hours. Macrophages were then activated with *C. acnes* (HL005PA1) for 24 hours. Antimicrobial activity was calculated by subtracting 24-hour CFU (colony counting unit) count with 1-hour CFU count and divide by CFU at 24-hour to determine the percentage of killing. Results are shown as mean ± SEM (n=7). P-values were calculated using unpaired Student's t-test of the antimicrobial activity of IFN-γ + LPS or M-CSF macrophages against *C. acnes* strains compared to the antimicrobial activity of IFN-γ + LPS with squalene or M-CSF with squalene against *C. acnes*. * = p-value < 0.05, ** = p-value < 0.01.

g. *C. acnes* were stimulated with diethylenetriamine NONOate (DETA NONOate), alkyl peroxide tertiary-butyl hydroperoxide (TBHP), and hydrogen peroxide (H2O2-) at varying concentration for 2 hours. CFUs were plotted for each concentration (n=3). P-values were calculated using unpaired Student's t-test of the *C. acnes* CFU of each treatment (DETA NONOate or TBHP) compared to the *C. acnes* CFU of H_2O_2. * = p-value < 0.05, ** = p-value < 0.01.

h. *C. acnes* were stimulated with alkyl peroxide tertiary-butyl hydroperoxide (TBHP) at varying concentration with media, N-acetyl cysteine (NAC), or squalene for 2 hours. CFUs were plotted for each concentration (n=3). P-values were calculated using unpaired Student's t-test of the *C. acnes* CFU of each treatment (NAC or squalene) compared to the *C. acnes* CFU of untreated. * = p-value < 0.05, ** = p-value < 0.01.
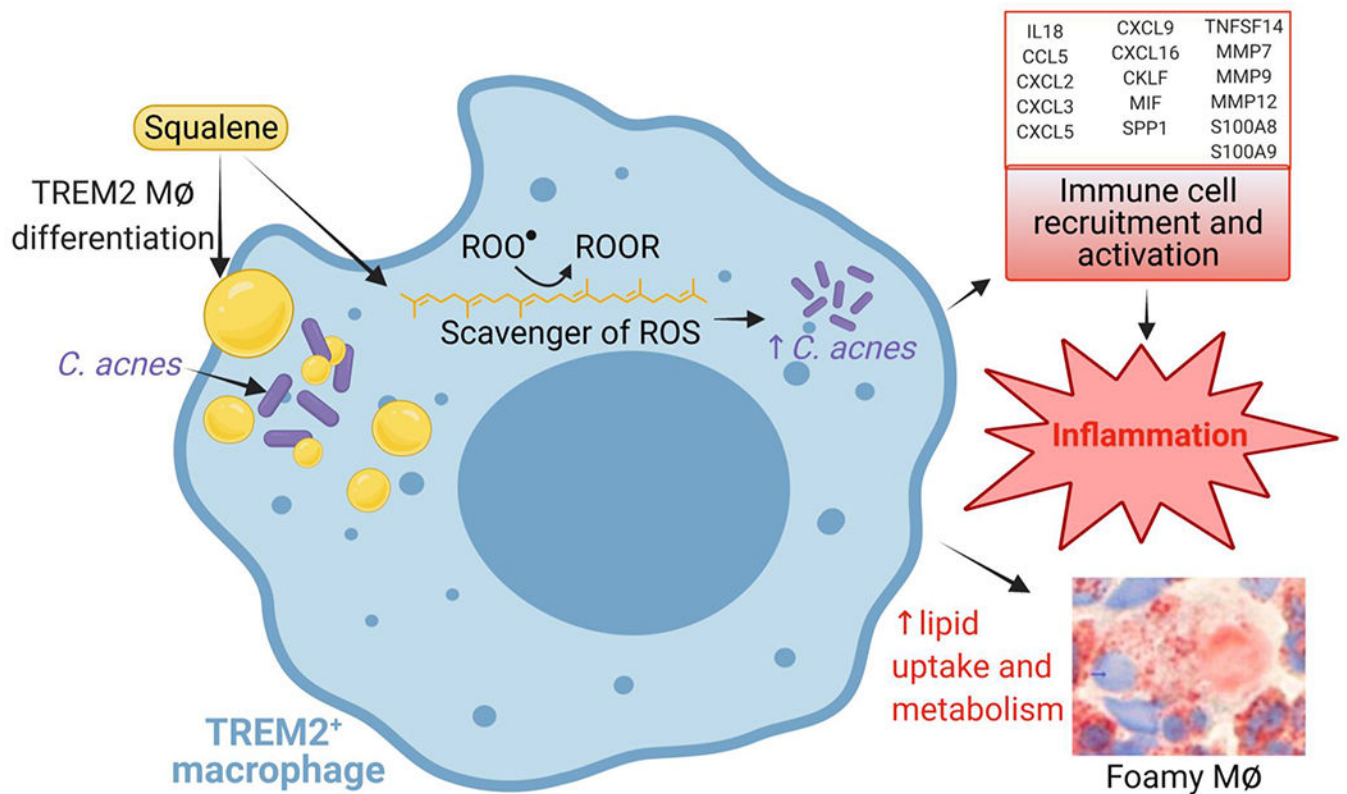
Fig. 5. Graphical Summary of Acne Inflammation with Squalene Upregulating TREM2 expression on Macrophages.

Our data showed that squalene, found abundant in acne lesions, upregulates the expression of TREM2 on macrophages. TREM2 expression enhances the phagocytic capacity of the macrophages to uptake lipids and bacteria, but do not have significant antimicrobial functions due to the ability of squalene to scavenge ROS (reactive oxygen species) as well as the downregulate enzymes in generation of reactive oxygen species and their response. Although squalene inhibits TREM2 macrophages antimicrobial activity, TREM2 macrophages contribute to inflammation by upregulating expression of pro-inflammatory chemokines, cytokines, MMPs, and S100 proteins to recruit and activate immune cells.